Southern blot analysis. An ES cell clone correctly targeting *Ifit1* was microinjected into C57BL/6 mouse blastocysts. Chimeric mice were mated with female C57BL/6 mice, and heterozygous F1 progenies were intercrossed to obtain *Ifit1*$^{-/-}$ mice.

Cells. HEK293T cells, Vero cells, and mouse embryonic fibroblasts (MEFs) were maintained in Dulbecco's modified Eagle's medium (Nakalai Tesque) supplemented with 10% fetal bovine serum (JRH Bioscience), 100 U/ml penicillin, and 100 μg/ml streptomycin (Gibco). MEFs were prepared from wild-type (WT) and *Ifit1*$^{-/-}$ day 14.5 embryos and immortalized by introduction of a plasmid encoding the simian virus 40 large T antigen. MEFs stably expressing Ifit1 were established by the previously described method with some modifications (34). In short, full-length cDNA of *Ifit1* was cloned into pMRX-puro (pMRX/*Ifit1*). Retrovirus was produced by introduction of pMRX/*Ifit1* into Plat-E packaging cells (35). MEFs were infected with the retrovirus, cultured in the presence of 1 μg/ml of puromycin (Sigma) for 5 days, and harvested for subsequent studies. To isolate peritoneal macrophages, mice were intraperitoneally injected with 5 ml of 4% thioglycolate medium (Sigma), and peritoneal exudative cells were isolated from the peritoneal cavity at 3 days postinjection. The cells were incubated for 2 h and then washed three times with Hanks' balanced salt solution. The remaining adherent cells were used as peritoneal macrophages in the experiments.

Viruses. Japanese encephalitis virus (JEV) strain AT31 (36) was used for the experiments. An NS5 K61A mutation of JEV was introduced into pMWATG1 (37) by PCR-based mutagenesis with the primers 5′-GCGAGGCTCAGCAGCTCTCCGTTGGCTCG-3′ and 5′-CGAGCCAACGGAGAGCTGCTGAGCCTCGC-3′ (the mutagenesis site is underlined) and verified by DNA sequencing. A recombinant virus, the JEV K61A mutant, was generated from pMWJEATG1/JEV K61A as previously described (36). MEFs or macrophages were infected with JEV at specified multiplicities of infection (MOIs). The virus yields in the culture supernatants were titrated by focus-forming assays on Vero cells and expressed as the number of focus-forming units (FFU), as previously described (38). The virus RNA accumulations in the JEV-infected cells were determined by real-time reverse transcription-PCR (RT-PCR) with primers targeting JEV NS5, normalized to the level of host GAPDH (glyceraldehyde-3-phosphate dehydrogenase), and expressed as the fold change in *Ifit1*$^{-/-}$ cells versus wild-type cells (value for wild type = 1).

Preparation of RNA. The 5′-terminal 200 nucleotides of the JEV genome were amplified by PCR using pMWATG1 (37) with the primers 5′-TAATACGACTCACTATTAGAAGTTTATCT-3′ (the T7 class II promoter sequence is underlined) and 5′-CATTACTACCCTCTTCACTCCCACTAGTGG-3′, and the luciferase reporter gene (*luc2*) was amplified using pGL4.14 (Promega) with the primers 5′-TAATACGACTCACTATAGGCCACCATGGAAGATGCCAAAAA-3′ (the T7 class III promoter sequence is underlined) and 5′-TACCACATTTGTAGAGGTTTTACTTGCTTT-3′. Subsequently, the PCR products were *in vitro* transcribed under the control of the T7 promoter with MEGAScript (Ambion). Biotin-labeled RNA was prepared by *in vitro* transcription in the presence of biotin-labeled UTP (PerkinElmer). Capped RNA substrates were produced with a ScriptCap 7-methylguanosine (m7G) capping system (Epicentre) in the presence (5′ cap positive [5′ cap$^+$]/2′-O Me positive [2′-O Me$^+$]) or absence (5′ cap$^+$/2′-O Me negative [2′-O Me$^-$]) of a ScriptCap vaccinia virus 2′-O MTase (Epicentre). ^{32}P-labeled m7GpppA-RNA substrate was prepared with a ScriptCap m7G capping system in the presence of ^{32}P-labeled GTP. A 5′ OH-RNA substrate was produced by incubating *in vitro*-transcribed RNA with calf intestinal alkaline phosphatase (CIAP) for 3 h at 37°C. All RNA substrates were purified with an RNeasy minikit (Qiagen) and stored at −80°C until use.

Real-time RT-PCR. Total RNA was isolated with the TRIzol reagent (Invitrogen), and 1 to 2 μg of RNA was reverse transcribed using Moloney murine leukemia virus reverse transcriptase (Promega) and random primers (Toyobo) after treatment with RQ1 DNase I (Promega). Real-time RT-PCR was performed in an ABI 7300 apparatus (Applied Biosystems) using a GoTaq real-time PCR system (Promega). All values were normalized by the expression of the GAPDH gene. The following primer sets were used: for the JEV NS5 gene, 5′-AACGCACATTACGCGTCCTAGAGATGA-3′ and 5′-CTAACCCAATACATCTCGTGATTGGAGTT-3′; for *Ifnb*, 5′-GGAGATGACGGAGAAGATGC-3′ and 5′-CCCAGTGCTGGAGAAATTGT-3′; for *luc2*, 5′-CCATTCTACCCACTCGAAGACG-3′ and 5′-CGTAGGTAATGTCCACCTCGA-3′; and for the GAPDH gene, 5′-CCTCGTCCCGTAGACAAAATG-3′ and 5′-TCTCCACTTTGCCACTGCAA-3′.

Recombinant proteins. Wild-type and K61A mutant JEV N-terminal NS5 (MTase domain) cDNAs were obtained by PCR using pMWATG1 with the primers 5′-GGATCCGGAAGGCCTGGGGGCAGGACGCTA-3′ and 5′-CTCGAGATGCTCAGGGTCTTTGTGCCACGT-3′. Full-length murine *Ifit1* cDNA and JEV MTase cDNA were inserted into pET-15b and pGEX-6P, respectively. pET/*Ifit1* and pGEX/JEV MTases were transformed into the *Escherichia coli* BL21(DE3) strain. Expression of the Ifit1 and JEV NS5 proteins was induced by addition of 0.5 mM isopropyl-1-thio-β-D-galactopyranoside (IPTG), and the expressed Ifit1 and JEV MTase proteins were purified using Ni^{2+}-affinity chromatography (Novagen) and glutathione-Sepharose 4B (Amersham Biosciences), respectively, according to each manufacturer's instructions. The purified protein was desalted and concentrated using an Amicon Ultra centrifugal filter unit (Millipore) and stored at −80°C until use.

***In vitro* MTase activity assay.** The MTase reaction was performed in a 20-μl reaction mixture of 50 mM Tris-HCl (pH 8.0), 6 mM KCl, 1.25 mM $MgCl_2$, and 0.5 mM *S*-adenosylmethionine (AdoMet) containing 10 nmol of ^{32}P-labeled m7GpppA-RNA substrate (JEV 5′-terminal 200 nucleotides) and 30 pmol of JEV MTase or 80 units of vaccinia virus 2′-O MTase (Epicentre) for 3 h at 37°C. The RNA was purified by passage through a postreaction cleanup column (Sigma) and digested with 10 U of nuclease P1 (Wako) in 50 mM sodium acetate overnight at 37°C. The samples were analyzed on thin-layer chromatography polyethyleneimine (PEI)-cellulose plates developed with 0.3 M ammonium sulfate.

RNA EMSAs. RNA electrophoretic mobility shift assays (EMSAs) were performed using a LightShift chemiluminescent RNA EMSA kit (Thermo Scientific) according to the manufacturer's instructions. Briefly, 0 to 20 pmol of recombinant murine Ifit1 and 2.5 pmol of *in vitro*-transcribed and biotin-labeled RNA were coincubated for 30 min at room temperature in RNA EMSA binding buffer (10 mM HEPES, pH 7.3, 20 mM KCl, 1 mM $MgCl_2$, 1 mM dithiothreitol, 0.1 μg/μl of yeast tRNA, 2% glycerol). The resulting Ifit1/RNA complexes were electrophoresed in a 7.5% native polyacrylamide gel. The separated RNAs were transferred to a positively charged nylon membrane and cross-linked at 120 mJ/cm^2 and an absorbance of 254 nm. The membrane was incubated with stabilized streptavidin-horseradish peroxidase conjugate (1:300 dilution; a component of the EMSA kit), and the bound stable peroxide was detected with luminol/enhancer solution (another component of the EMSA kit). The gel-shift band intensities were quantified using ImageJ software (National Institutes of Health).

RNA pulldown assay. For RNA pulldown assays, an expression vector for hemagglutinin (HA)-tagged murine full-length Ifit1 was transfected into HEK293T cells using Lipofectamine 2000 (Invitrogen). The *Ifit1*-transfected cells were lysed in RNA-binding buffer (10 mM HEPES, pH 7.3, 500 mM KCl, 1 mM EDTA, 2 mM $MgCl_2$, 0.1% NP-40, 0.1 μg/μl of yeast tRNA (Ambion), 1 U/ml of RNase inhibitor [Toyobo]), and the lysate (200 μg) was coincubated with 25 pmol of biotin-labeled RNA and streptavidin-agarose (Invitrogen) in RNA-binding buffer for 30 min at room temperature. The binding complexes were washed five times with RNA-binding buffer, followed by SDS-PAGE and immunoblotting with an anti-HA probe (F-7) antibody (Santa Cruz Biotechnology). The intensity of the detected Ifit1 band was quantified using ImageJ software (National Institutes of Health).

RNA immunoprecipitation. RNA immunoprecipitation was performed as described previously (38) with slight modifications. MEFs (2×10^5) stably expressing Flag-tagged Ifit1 were infected with JEV at an MOI of 1.0 and cultured for 24 h. The cells were then lysed in 500 μl of RNA

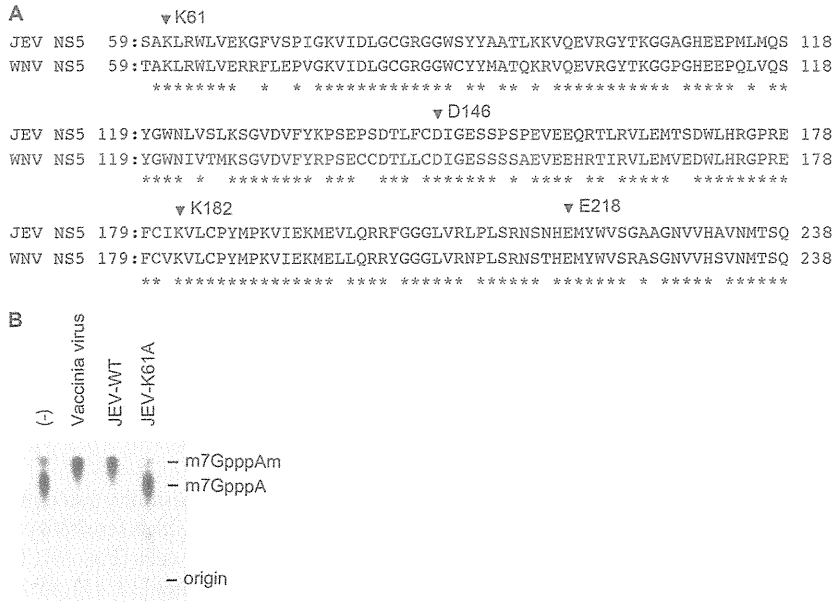

FIG 1 Generation of an MTase-defective JEV mutant. (A) Sequence homology between NS5 proteins of JEV (AT31 strain, GenBank accession number AB196926) and WNV (00-3356 strain, GenBank accession number EF530047). Arrowheads, MTase catalytic K-D-K-E tetrad; *, consensus sequences between the two proteins. (B) 2′-O MTase activity of JEV WT and JEV K61A mutant recombinant NS5 proteins by thin-layer chromatography assays. The substrate m7GpppA-RNA (^{32}P-labeled JEV 5′-terminal 200 nucleotides) was methylated *in vitro* with the respective recombinant NS5 proteins or vaccinia virus 2′-O MTase, digested with P1 nuclease, and developed on PEI-cellulose plates. The positions of 2′-O methylated (m7GpppAm) and unmethylated (m7GpppA) RNA are indicated. Data are representative of four independent experiments.

buffer (10 mM HEPES, pH 7.3, 500 mM KCl, 1 mM EDTA, 2 mM $MgCl_2$, 0.1% NP-40, 0.1 μg/μl of yeast tRNA (Ambion), 1 U/ml of RNase inhibitor [Toyobo], 1 tablet/10 ml of Complete mini-protease inhibitor cocktail [Roche]). After centrifugation at 15,000 rpm for 20 min at 4°C, 50-μl aliquots of the supernatants were recovered as input samples and the remaining supernatants were precleared with 30 μl of 50% protein G-conjugated Sepharose and 1 μg of mouse normal IgG for 1 h. After centrifugation of the beads, the supernatants were immunoprecipitated with 1 μg of mouse normal IgG or anti-Flag M2 antibody (Santa Cruz Biotechnology) and 30 μl of 50% protein G-conjugated Sepharose. The beads were washed five times with RNA buffer without yeast tRNA, and RNA was isolated from the precipitants and input samples with the TRIzol reagent. The RNA was reverse transcribed as described above and subjected to the first round of PCR with JEV NS1-specific primers 5′-TCTG TCACTAGACTGGAGCA-3′ and 5′-CCAGAAACATCACCAGAAGG-3′. The PCR products were then analyzed by quantitative PCR with nested primers 5′-GAGCACTGACGAGTGTGATG-3′ and 5′-AGCGACTCTC AATCCAGTAC-3′. All values were normalized by the values for the input samples (indicated as percent input).

Cellular translational reporter assay. MEFs (2×10^5) were pretreated with 1,000 U/ml of universal type I interferon (PBL Biomedical Laboratories) for 6 h. Three types of 5′ modified luciferase mRNAs (2 μg of 5′-PPP, 5′ cap$^+$/2′-O Me$^-$, and 5′ cap$^+$/2′-O Me$^+$) were transiently transfected into MEFs using the Lipofectamine 2000 reagent (Invitrogen) according to the manufacturer's instructions. At 6 h after the transfection, RNA was isolated and analyzed for the quantity of the luciferase mRNAs (*luc2*). The luciferase activities of whole-cell lysates were measured using a dual-luciferase reporter assay system (Promega). The numbers of relative light units (RLU) were normalized by the concentrations of proteins determined by use of a bicinchoninic acid protein assay kit (Thermo Scientific).

Statistical analysis. Statistical analyses were conducted on each independent data set. An unpaired Student's *t* test was used to determine the statistical significance of differences in the experimental data. *P* values of <0.05 were considered to indicate statistical significance.

RESULTS

***Ifit1*$^{-/-}$ cells fail to restrict the replication of a mutant JEV lacking 2′-O MTase activity.** Previous analysis of the flavivirus West Nile virus (WNV) 2′-O MTase revealed residues in NS5 (K61, D146, K182, and E218) that were essential for its biochemical activity (8). A WNV mutant (E218A) lacking 2′-O MTase activity was attenuated in mouse MEFs and macrophages but showed enhanced replication in *Ifit1*$^{-/-}$ cells (13, 15). As NS5 is a highly conserved protein in flaviviruses, the four residues integral to the 2′-O MTase activity are identical in WNV and JEV (Fig. 1A). Replacement of lysine 61 by alanine in the JEV NS5 MTase domain (JEV K61A) abolished the JEV 2′-O MTase activity *in vitro* (Fig. 1B). We generated *Ifit1*$^{-/-}$ mice (Fig. 2A to C) and infected MEFs with JEV WT and JEV K61A strains (Fig. 3A). The JEV WT replicated equivalently in wild-type and *Ifit1*$^{-/-}$ MEFs. In comparison, the production of the JEV K61A mutant was decreased in wild-type MEFs, suggesting that 2′-O MTase activity is required for JEV replication. Consistent with this and analogous studies with an WNV E218A strain (13), replication of the JEV K61A strain was enhanced (approximately 173-fold increased at 4 days postinfection; $P < 0.05$) in *Ifit1*$^{-/-}$ MEFs compared with wild-type MEFs. We also infected peritoneal macrophages with JEV WT and JEV K61A strains (Fig. 3B). Similar to the results obtained with MEFs, replication of the JEV WT was similarly observed in wild-type and *Ifit1*$^{-/-}$ macrophages. However, replication of the JEV K61A mutant was severely decreased in wild-type but not *Ifit1*$^{-/-}$ macrophages, and the virus was not detected at 4 days postinfection in wild-type cells. For further confirmation, we analyzed virus RNA accumulation at 4 days postinfection (Fig. 3C and D). Whereas RNA levels of JEV WT were similar in wild-type and *Ifit1*$^{-/-}$ MEFs, those of the JEV K61A mutant were markedly

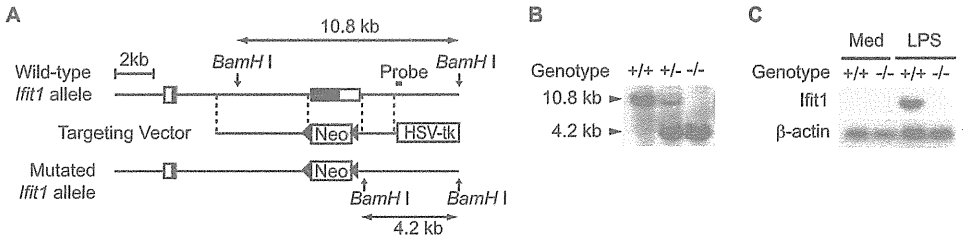

FIG 2 Generation of *Ifit1*$^{-/-}$ mice. (A) Schematic representation of the *Ifit1* gene-targeting strategies. Solid boxes, coding regions of the *Ifit1* gene; open boxes, untranslated regions; Neo and HSV tk, a neomycin-resistance gene cassette and a herpes simplex virus thymidine kinase gene, respectively. The positions of the probe and restriction enzyme site for Southern blotting are shown. (B) Genomic DNA was isolated from the tails of wild-type (+/+), heterozygous (+/-), and homozygous (−/−) *Ifit1* mutant mice. A Southern blot analysis performed after digestion of the genomic DNA with BamHI shows the correct targeting of the locus. (C) Peritoneal exudative macrophages were harvested from wild-type (+/+) or *Ifit1*-deficient (−/−) mice. Total RNA (10 μg) was blotted onto a nylon membrane, and Ifit1 and β-actin mRNA expression was detected by Northern blot analysis with the respective cDNA probes. LPS lanes, cells stimulated with 100 ng/ml of lipopolysaccharide for 4 h to induce endogenous Ifit1 expression; Med lanes, cells treated with medium alone.

higher (approximately 13-fold; $P < 0.05$) in *Ifit1*$^{-/-}$ MEFs than in wild-type MEFs. To further corroborate these findings, we reintroduced the *Ifit1* gene into *Ifit1*$^{-/-}$ MEFs using a retrovirus vector. Replication of the JEV K61A mutant was considerably suppressed (approximately 4-fold; $P < 0.05$) by ectopic Ifit1 expression in *Ifit1*$^{-/-}$ MEFs (Fig. 3E). *Ifnb* was similarly induced in wild-type and *Ifit1*$^{-/-}$ MEFs after infection with the JEV K61A mutant, excluding the possibility that defective type I IFN production is responsible for the high sensitivity to infection with the JEV K61A mutant in *Ifit1*$^{-/-}$ cells (Fig. 3F). Thus, consistent with the findings of previous studies (13, 15), Ifit1 inhibits replication and infection of flavivirus mutants that lack 2′-O MTase activity.

Ifit1 preferentially binds to virus RNA lacking 2′-O methylation. Next, we analyzed how Ifit1 recognizes 2′-O MTase mutant

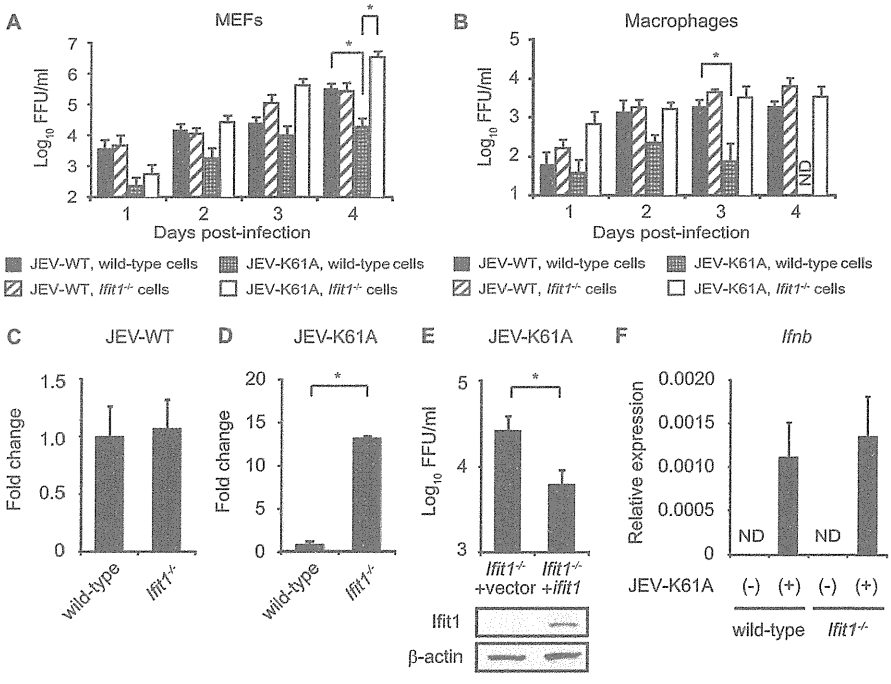

FIG 3 *Ifit1*$^{-/-}$ MEFs and macrophages fail to restrict the replication of the 2′-O MTase mutant JEV. (A, B) Culture supernatants of wild-type and *Ifit1*$^{-/-}$ MEFs (A) and macrophages (B) infected with JEV WT and the JEV K61A mutant (MOIs, 0.1 for MEFs and 0.5 for macrophages) were harvested at the indicated days postinfection. The virus titers in 1-ml supernatant aliquots were determined by focus-forming assays on Vero cells and expressed as the $\log_{10}$ number of FFU/ml. Data are shown as means ± SDs of quadruplicate samples generated from four independent experiments with statistical significance. ND, not detected. *, $P < 0.05$. (C, D) Accumulation of JEV WT (C) and the JEV K61A mutant (D) RNA in wild-type and *Ifit1*$^{-/-}$ MEFs at 4 days postinfection determined by quantitative real-time RT-PCR. JEV NS5 RNA levels were normalized to the level of host GAPDH and are expressed as the fold change in *Ifit1*$^{-/-}$ cells versus wild-type cells (value for wild type = 1). Data are representative of three independent experiments with statistical significance. *, $P < 0.05$. (E) Culture supernatants of vector-transduced (+vector) and Flag-tagged *Ifit1* gene-transduced (+*Ifit1*) *Ifit1*$^{-/-}$ MEFs infected with the JEV K61A mutant (MOI, 0.1) were harvested at 3 days postinfection. The virus titers in 1-ml supernatant aliquots were determined by focus-forming assays on Vero cells and expressed as the $\log_{10}$ number of FFU/ml. Expression of Ifit1 and β-actin determined by immunoblotting with anti-Flag or anti-β-actin antibodies is shown at the bottom. Data are representative of three independent experiments. *, $P < 0.05$. (F) Wild-type and *Ifit1*$^{-/-}$ MEFs were infected with the JEV K61A mutant (MOI, 0.1). At 4 days postinfection, cells were harvested and analyzed for *Ifnb* expression by quantitative RT-PCR. *Ifnb* RNA levels were expressed relative to those of GAPDH. ND, not detected. Data are shown as means ± SDs and are representative of data from three independent experiments.

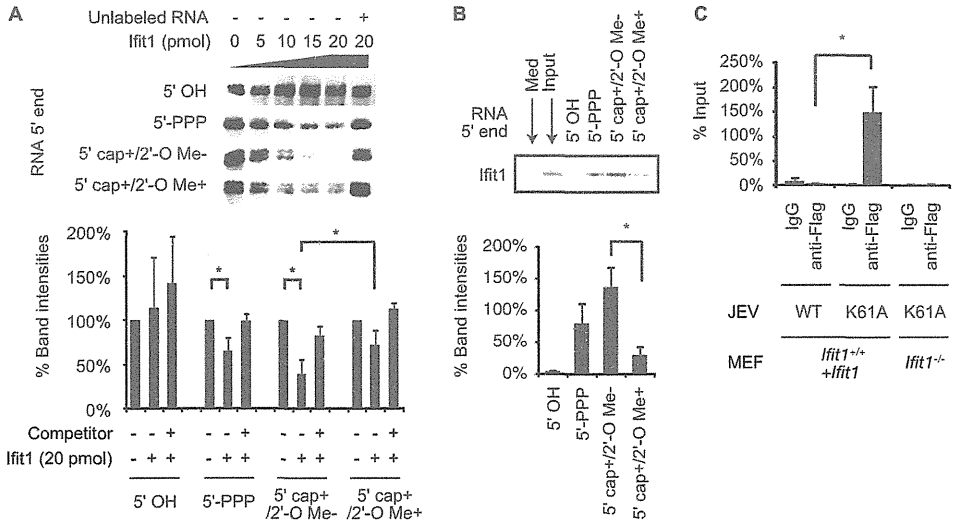

FIG 4 Ifit1 preferentially binds to virus RNA lacking 2′-O methylation. (A) Electrophoretic mobility shift of biotin-labeled RNA (JEV 5′-terminal 200 nucleotides) with recombinant Ifit1. The presence or absence of a 5′ cap and 2′-O Me of the JEV 5′-terminal 200 nucleotides is indicated. Unlabeled 5′-PPP RNA was used as a competitor. The loss of the band indicates binding of RNA and Ifit1 (top). The band intensities (in percent) calculated by ImageJ are shown at the bottom. Data are representative (top) and means ± SDs (bottom) of five independent experiments. *, $P < 0.05$. (B) Lysates from HEK293T cells transfected with HA-tagged Ifit1 were incubated with 2.5 pmol of biotin-labeled RNA. The presence or absence of a 5′ cap and 2′-O Me of the JEV 5′-terminal 200 nucleotides is indicated. 5′ OH RNA was produced by incubating *in vitro*-transcribed RNA with CIAP. RNA was incubated with streptavidin beads, and the precipitates were separated by SDS-PAGE and immunoblotted with an anti-HA antibody (top). Med and Input, samples from whole-cell lysates of empty vector- and *Ifit1*-transfected 293T cells, respectively. The percent band intensities calculated by ImageJ are shown at the bottom. Data are representative (top) and means ± SDs (bottom) of three independent experiments. *, $P < 0.05$. (C) MEFs stably expressing Ifit1 (*Ifit1*$^{+/+}$ + *Ifit1*) or *Ifit1*$^{-/-}$ MEFs were infected with JEV WT or the JEV K61A mutant at an MOI of 1.0. The cells were harvested after 24 h, and JEV RNA/Ifit1-binding complexes were immunoprecipitated with a mouse anti-Flag antibody or mouse IgG. The immunoprecipitated RNA was analyzed by nested RT-PCR using primers that detect the JEV NS1 gene. Each value was normalized by the value for the input (indicated in percent). Data are means ± SDs of three independent experiments. *, $P < 0.05$.

viruses. While recombinant IFIT1 reportedly binds to 5′-PPP RNA (32), the mRNA of the JEV K61A mutant has a 5′ m7G cap but lacks 2′-O methylation (5′ cap$^+$/2′-O Me$^-$). We examined whether Ifit1 can also interact directly with 5′ cap$^+$/2′-O Me$^-$ RNA using electrophoretic mobility shift assays. Consistent with a previous report (32), bands of 5′-PPP RNA but not RNA lacking phosphate at the 5′ end (5′ OH) were diminished after addition of recombinant Ifit1 (Fig. 4A). Furthermore, Ifit1 blocked the electrophoretic mobility of the 5′ cap$^+$/2′-O Me$^-$ RNA. However, this effect was rescued by exogenous addition *in vitro* of 2′-O methylation (5′ cap$^+$/2′-O Me$^+$). The efficient binding of Ifit1 to 5′ cap$^+$/2′-O Me$^-$ RNA was corroborated by RNA pulldown assays (Fig. 4B). HA-tagged Ifit1 was expressed in HEK293T cells, and cell lysates were incubated with biotin-labeled *in vitro*-transcribed RNA and streptavidin-agarose. Then, binding complexes of Ifit1/RNA were analyzed by Western blotting. While Ifit1 was not pulled down with 5′ OH RNA, modest binding of Ifit1 to 5′-PPP RNA and 5′ cap$^+$/2′-O Me$^+$ RNA was observed. In comparison, the strongest Ifit1 protein signal was observed with 5′ cap$^+$/2′-O Me$^-$ RNA. These findings suggest that Ifit1 preferentially binds to 5′ capped RNA lacking 2′-O methylation.

To confirm independently that Ifit1 interacts with 5′ capped RNA lacking 2′-O methylation, we performed RNA immunoprecipitation assays using cell lysates from JEV-infected MEFs that ectopically expressed a Flag-tagged Ifit1. After immunoprecipitation with an anti-Flag antibody, the JEV mRNA was measured by nested RT-PCR analysis (Fig. 4C). JEV RNA was only marginally detected in lysates precipitated with control IgG and lysates of *Ifit1*$^{-/-}$ MEFs infected with the JEV K61A mutant, indicating the specificity of Ifit1 binding in the assay. Virus RNA in JEV K61A mutant-infected MEFs was detected at a level over 37-fold higher than that in JEV WT-infected MEFs. Taken together, these findings suggest that Ifit1 directly interacts with virus mRNA lacking 2′-O methylation.

Ifit1 selectively inhibits translation of 5′ capped 2′-O unmethylated mRNA. To examine the mechanism by which Ifit1 exerts an antiviral effect by associating with mRNA lacking 2′-O methylation, we used a luciferase translational reporter assay. Luciferase RNAs with different 5′ structures were transfected into type I IFN-primed MEFs, and total RNA and cell lysates were harvested 6 h later. Importantly, the levels of luciferase RNAs in wild-type and *Ifit1*$^{-/-}$ cells were unaffected by any of the 5′ modifications (Fig. 5A). We then analyzed the translational efficiency of the transfected RNAs by measuring the luciferase activity (Fig. 5B). As expected (1), uncapped 5′-PPP luciferase mRNA was not translated in either wild-type or *Ifit1*$^{-/-}$ MEFs. Capping of the mRNA (5′ cap$^+$/2′-O Me$^-$) increased translation in wild-type cells, although the levels were profoundly lower ($P < 0.05$) than those in *Ifit1*$^{-/-}$ cells. In comparison, addition of 2′-O methylation to the 5′ cap (5′ cap$^+$/2′-O Me$^+$) *in vitro* resulted in similar levels of translation in wild-type and *Ifit1*$^{-/-}$ MEFs. Even in MEFs that were not treated with type I IFN, similar patterns of luciferase activity were observed (Fig. 5C), indicating that slightly expressed Ifit1 might contribute to the inhibition. Taken together, our data establish that Ifit1 preferentially binds to 5′ capped mRNA lacking 2′-O methylation and inhibits its translation.

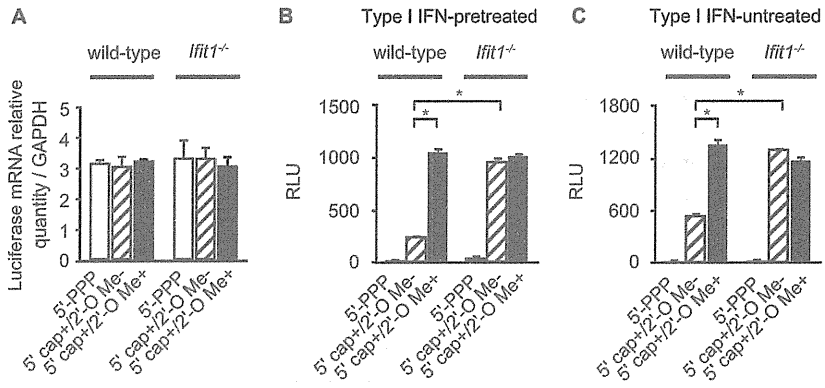

FIG 5 Ifit1 selectively inhibits the translation of mRNA lacking 2′-O methylation. (A) The luciferase RNA amounts at 6 h after RNA transfection were determined by quantitative real-time RT-PCR. The relative luciferase mRNA amounts, calculated as the amount of each transfected mRNA (*luc2*) divided by the level of GAPDH mRNA expression, are shown. The presence or absence of a 5′ cap and 2′-O Me of the introduced luciferase RNA is indicated. Data are shown as means ± SDs and are representative of three independent experiments. (B, C) Wild-type and *Ifit1*$^{-/-}$ MEFs pretreated with type I IFN (B) or untreated (C) were transiently transfected with luciferase mRNA. Luciferase activities were measured at 6 h after the transfection and are shown as relative light units (RLU). The presence or absence of a 5′ cap and 2′-O Me of the introduced luciferase RNA is indicated. Data are shown as means ± SDs of triplicate samples of the representative results. Similar results were obtained in three independent experiments. *, $P < 0.05$.

DISCUSSION

In this study, we investigated the mechanisms by which Ifit1 recognizes RNA of JEV lacking 2′-O MTase activity. Ifit1 inhibited the translation of mRNA through association with mRNA lacking 2′-O methylation.

To analyze the role of Ifit1 in 5′ cap structure-dependent antiviral responses, we generated a JEV MTase mutant. The K61, D146, K182, and E218 residues have all been shown to be essential for the MTase activity of the NS5 protein and replication of WNV (8, 11). While a WNV E218A mutant was previously used for analysis of Ifit1-mediated antiviral responses (13), in our assays, the corresponding JEV E218A mutant was severely impaired in replication in Vero cells and rapidly reverted to the wild type during cell culture, preventing its use (data not shown). A similar phenotype was observed with the WNV D146A 2′-O methylation mutant (11). However, unlike our results, it has recently been reported that a JEV E218A mutant is stable in Vero cells (39). This would be due to the different strains used in the two studies. Thus, mutation of residues that are essential for the 2′-O MTase activity of a flavivirus NS5 protein can differentially impact replication of JEV and WNV even in cells lacking type I IFN responses and IFIT1 expression.

Previous *in vitro* studies indicated that IFIT family proteins bind to several types of RNA, including 5′-PPP RNA and AU-rich double-stranded RNA (31, 32). Indeed, an analysis of the IFIT2 crystal structure indicated the presence of a positively charged RNA-binding channel (31), findings which were supported by the X-ray crystallographic structure of complexes of 5′-PPP RNA with human IFIT5 (33, 40). We also observed that Ifit1 could bind to 5′-PPP RNA. However, our biochemical analysis showed that Ifit1 bound strongly to 5′ capped RNA lacking 2′-O methylation and addition of 2′-O methylation weakened the binding of Ifit1 to the RNA. Since mRNAs of virtually all higher eukaryotes are believed to be methylated at the ribose 2′-O position (41), this modification likely serves as a molecular pattern for discriminating self from nonself.

Although it remains unclear how 2′-O methylation reduces Ifit1 binding to RNA, structural changes to the RNA at the 5′ terminus after 2′-O methylation could sterically hamper Ifit1 binding. The crystal structure of the 5′-PPP RNA/IFIT5 complex has indicated that the RNA-binding site on human IFIT5 is located in a narrow pocket, thus raising the possibility that 5′ capped and 2′-O methylated RNA cannot fit within an analogous pocket of Ifit1 due to a size limitation (33). Future structural analyses of the binding complex of 5′ capped RNA with Ifit1 will be required to reveal the precise mechanisms by which Ifit1 recognizes 5′ capped RNA lacking 2′-O methylation. Additional studies must also test whether other IFITs preferentially associate with 5′ capped RNA lacking 2′-O methylation.

Ifit1 also has an antiviral activity against several negative-stranded viruses, such as vesicular stomatitis virus (VSV) and parainfluenza virus type 5 (PIV5) (32, 42), whose mRNAs are 2′-O methylated (6, 42). In this regard, Ifit1 is supposed to have an antiviral effect independent of 2′-O methylation. Indeed, IFIT1 is able to bind 5′-PPP genomic RNA (32).

Given the previous and present findings that Ifit1 inhibits mRNA translation (23–26), our data are most consistent with a model in which Ifit1 restricts replication of viruses with 5′ capped RNA lacking 2′-O methylation through direct RNA binding and subsequent inhibition of translation. Human IFIT1 and murine Ifit1 were previously reported to interact with eIF3 to interfere with translation (23–26), and replication of hepatitis C virus, whose RNA lacks a 5′ cap, was also impaired by IFIT1 through binding to eIF3 (43). Thus, Ifit1 may associate with both eIF3 and virus mRNA to inhibit translation and infection.

The Ifit family proteins consist of several conserved members. However, Ifit1 and Ifit2 appear to have distinct antiviral activities (44). Thus, the nonredundant and redundant roles of the Ifit family proteins remain to be elucidated. Generation of mice lacking the other members or all of the Ifit family proteins will be useful to reveal the physiological functions.

ACKNOWLEDGMENTS

We thank M. S. Diamond for fruitful discussions and suggestions, T. Wakita for providing us with the JEV AT31 strain, and T. Kitamura for providing us with Plat-E cells. We also thank Y. Magota for technical assistance, C. Hidaka for excellent secretarial assistance, and members of the K. Takeda laboratory for discussions.

This work was supported by grants from the Ministry of Education, Culture, Sports, Science and Technology, the Japan Science and Technology Agency, and The Osaka Foundation for Promotion of Clinical Immunology.

REFERENCES

1. Muthukrishnan S, Both GW, Furuichi Y, Shatkin AJ. 1975. 5′-Terminal 7-methylguanosine in eukaryotic mRNA is required for translation. Nature 255:33–37.
2. Furuichi Y, LaFiandra A, Shatkin AJ. 1977. 5′-Terminal structure and mRNA stability. Nature 266:235–239.
3. Belanger F, Stepinski J, Darzynkiewicz E, Pelletier J. 2010. Characterization of hMTr1, a human Cap1 2′-O-ribose methyltransferase. J. Biol. Chem. 285:33037–33044.
4. Werner M, Purta E, Kaminska KH, Cymerman IA, Campbell DA, Mittra B, Zamudio JR, Sturm NR, Jaworski J, Bujnicki JM. 2011. 2′-O-Ribose methylation of cap2 in human: function and evolution in a horizontally mobile family. Nucleic Acids Res. 39:4756–4768.
5. Both GW, Furuichi Y, Muthukrishnan S, Shatkin AJ. 1975. Ribosome binding to reovirus mRNA in protein synthesis requires 5′ terminal 7-methylguanosine. Cell 6:185–195.
6. Abraham G, Rhodes DP, Banerjee AK. 1975. The 5′ terminal structure of the methylated mRNA synthesized in vitro by vesicular stomatitis virus. Cell 5:51–58.
7. Salas ML, Kuznar J, Vinuela E. 1981. Polyadenylation, methylation, and capping of the RNA synthesized in vitro by African swine fever virus. Virology 113:484–491.
8. Ray D, Shah A, Tilgner M, Guo Y, Zhao Y, Dong H, Deas TS, Zhou Y, Li H, Shi PY. 2006. West Nile virus 5′-cap structure is formed by sequential guanine N-7 and ribose 2′-O methylations by nonstructural protein 5. J. Virol. 80:8362–8370.
9. Decroly E, Imbert I, Coutard B, Bouvet M, Selisko B, Alvarez K, Gorbalenya AE, Snijder EJ, Canard B. 2008. Coronavirus nonstructural protein 16 is a cap-0 binding enzyme possessing (nucleoside-2′O)-methyltransferase activity. J. Virol. 82:8071–8084.
10. Morin B, Coutard B, Lelke M, Ferron F, Kerber R, Jamal S, Frangeul A, Baronti C, Charrel R, de Lamballerie X, Vonrhein C, Lescar J, Bricogne G, Gunther S, Canard B. 2010. The N-terminal domain of the arenavirus L protein is an RNA endonuclease essential in mRNA transcription. PLoS Pathog. 6:e1001038. doi:10.1371/journal.ppat.1001038.
11. Zhou Y, Ray D, Zhao Y, Dong H, Ren S, Li Z, Guo Y, Bernard KA, Shi PY, Li H. 2007. Structure and function of flavivirus NS5 methyltransferase. J. Virol. 81:3891–3903.
12. Dong H, Zhang B, Shi PY. 2008. Flavivirus methyltransferase: a novel antiviral target. Antiviral Res. 80:1–10.
13. Daffis S, Szretter KJ, Schriewer J, Li J, Youn S, Errett J, Lin TY, Schneller S, Zust R, Dong H, Thiel V, Sen GC, Fensterl V, Klimstra WB, Pierson TC, Buller RM, Gale M, Jr, Shi PY, Diamond MS. 2010. 2′-O methylation of the viral mRNA cap evades host restriction by IFIT family members. Nature 468:452–456.
14. Zust R, Cervantes-Barragan L, Habjan M, Maier R, Neuman BW, Ziebuhr J, Szretter KJ, Baker SC, Barchet W, Diamond MS, Siddell SG, Ludewig B, Thiel V. 2011. Ribose 2′-O-methylation provides a molecular signature for the distinction of self and non-self mRNA dependent on the RNA sensor Mda5. Nat. Immunol. 12:137–143.
15. Szretter KJ, Daniels BP, Cho H, Gainey MD, Yokoyama WM, Gale M, Jr, Virgin HW, Klein RS, Sen GC, Diamond MS. 2012. 2′-O methylation of the viral mRNA cap by West Nile virus evades ifit1-dependent and -independent mechanisms of host restriction in vivo. PLoS Pathog. 8:e1002698. doi:10.1371/journal.ppat.1002698.
16. Colonno RJ, Stone HO. 1976. Newcastle disease virus mRNA lacks 2′-O-methylated nucleotides. Nature 261:611–614.
17. Barik S. 1993. The structure of the 5′ terminal cap of the respiratory syncytial virus mRNA. J. Gen. Virol. 74(Pt 3):485–490.
18. Der SD, Zhou A, Williams BR, Silverman RH. 1998. Identification of genes differentially regulated by interferon alpha, beta, or gamma using oligonucleotide arrays. Proc. Natl. Acad. Sci. U. S. A. 95:15623–15628.
19. Takaoka A, Yanai H. 2006. Interferon signalling network in innate defence. Cell. Microbiol. 8:907–922.
20. Fensterl V, Sen GC. 2011. The ISG56/IFIT1 gene family. J. Interferon Cytokine Res. 31:71–78.
21. Sen GC, Fensterl V. 2012. Crystal structure of IFIT2 (ISG54) predicts functional properties of IFITs. Cell Res. 22:1407–1409.
22. Diamond MS, Farzan M. 2013. The broad-spectrum antiviral functions of IFIT and IFITM proteins. Nat. Rev. Immunol. 13:46–57.
23. Hui DJ, Terenzi F, Merrick WC, Sen GC. 2005. Mouse p56 blocks a distinct function of eukaryotic initiation factor 3 in translation initiation. J. Biol. Chem. 280:3433–3440.
24. Terenzi F, Pal S, Sen GC. 2005. Induction and mode of action of the viral stress-inducible murine proteins, P56 and P54. Virology 340:116–124.
25. Terenzi F, Hui DJ, Merrick WC, Sen GC. 2006. Distinct induction patterns and functions of two closely related interferon-inducible human genes, ISG54 and ISG56. J. Biol. Chem. 281:34064–34071.
26. Fensterl V, White CL, Yamashita M, Sen GC. 2008. Novel characteristics of the function and induction of murine p56 family proteins. J. Virol. 82:11045–11053.
27. Li Y, Li C, Xue P, Zhong B, Mao AP, Ran Y, Chen H, Wang YY, Yang F, Shu HB. 2009. ISG56 is a negative-feedback regulator of virus-triggered signaling and cellular antiviral response. Proc. Natl. Acad. Sci. U. S. A. 106:7945–7950.
28. Liu XY, Chen W, Wei B, Shan YF, Wang C. 2011. IFN-induced TPR protein IFIT3 potentiates antiviral signaling by bridging MAVS and TBK1. J. Immunol. 187:2559–2568.
29. Xiao S, Li D, Zhu HQ, Song MG, Pan XR, Jia PM, Peng LL, Dou AX, Chen GQ, Chen SJ, Chen Z, Tong JH. 2006. RIG-G as a key mediator of the antiproliferative activity of interferon-related pathways through enhancing p21 and p27 proteins. Proc. Natl. Acad. Sci. U. S. A. 103:16448–16453.
30. Terenzi F, Saikia P, Sen GC. 2008. Interferon-inducible protein, P56, inhibits HPV DNA replication by binding to the viral protein E1. EMBO J. 27:3311–3321.
31. Yang Z, Liang H, Zhou Q, Li Y, Chen H, Ye W, Chen D, Fleming J, Shu H, Liu Y. 2012. Crystal structure of ISG54 reveals a novel RNA binding structure and potential functional mechanisms. Cell Res. 22:1328–1338.
32. Pichlmair A, Lassnig C, Eberle CA, Gorna MW, Baumann CL, Burkard TR, Burckstummer T, Stefanovic A, Krieger S, Bennett KL, Rulicke T, Weber F, Colinge J, Muller M, Superti-Furga G. 2011. IFIT1 is an antiviral protein that recognizes 5′-triphosphate RNA. Nat. Immunol. 12:624–630.
33. Abbas YM, Pichlmair A, Gorna MW, Superti-Furga G, Nagar B. 2013. Structural basis for viral 5′-PPP-RNA recognition by human IFIT proteins. Nature 494:60–64.
34. Yamamoto M, Okuyama M, Ma JS, Kimura T, Kamiyama N, Saiga H, Ohshima J, Sasai M, Kayama H, Okamoto T, Huang DC, Soldati-Favre D, Horie K, Takeda J, Takeda K. 2012. A cluster of interferon-gamma-inducible p65 GTPases plays a critical role in host defense against Toxoplasma gondii. Immunity 37:302–313.
35. Morita S, Kojima T, Kitamura T. 2000. Plat-E: an efficient and stable system for transient packaging of retroviruses. Gene Ther. 7:1063–1066.
36. Mori Y, Okabayashi T, Yamashita T, Zhao Z, Wakita T, Yasui K, Hasebe F, Tadano M, Konishi E, Moriishi K, Matsuura Y. 2005. Nuclear localization of Japanese encephalitis virus core protein enhances viral replication. J. Virol. 79:3448–3458.
37. Zhao Z, Date T, Li Y, Kato T, Miyamoto M, Yasui K, Wakita T. 2005. Characterization of the E-138 (Glu/Lys) mutation in Japanese encephalitis virus by using a stable, full-length, infectious cDNA clone. J. Gen. Virol. 86:2209–2220.
38. Katoh H, Mori Y, Kambara H, Abe T, Fukuhara T, Morita E, Moriishi K, Kamitani W, Matsuura Y. 2011. Heterogeneous nuclear ribonucleoprotein A2 participates in the replication of Japanese encephalitis virus through an interaction with viral proteins and RNA. J. Virol. 85:10976–10988.
39. Li SH, Dong H, Li XF, Xie X, Zhao H, Deng YQ, Wang XY, Ye Q, Zhu SY, Wang HJ, Zhang B, Leng QB, Zuest R, Qin ED, Qin CF, Shi PY. 2013. Rational design of a flavivirus vaccine by abolishing viral RNA 2′-O methylation. J. Virol. 87:5812–5819.
40. Katibah GE, Lee HJ, Huizar JP, Vogan JM, Alber T, Collins K. 2013. tRNA binding, structure, and localization of the human interferon-induced protein IFIT5. Mol. Cell 49:743–750.
41. Banerjee AK. 1980. 5′-terminal cap structure in eucaryotic messenger ribonucleic acids. Microbiol. Rev. 44:175–205.
42. Andrejeva J, Norsted H, Habjan M, Thiel V, Goodbourn S, Randall RE. 2013. ISG56/IFIT1 is primarily responsible for interferon-induced changes to patterns of parainfluenza virus type 5 transcription and protein synthesis. J. Gen. Virol. 94:59–68.
43. Wang C, Pflugheber J, Sumpter R, Jr, Sodora DL, Hui D, Sen GC, Gale M, Jr. 2003. Alpha interferon induces distinct translational control programs to suppress hepatitis C virus RNA replication. J. Virol. 77:3898–3912.
44. Fensterl V, Wetzel JL, Ramachandran S, Ogino T, Stohlman SA, Bergmann CC, Diamond MS, Virgin HW, Sen GC. 2012. Interferon-induced Ifit2/ISG54 protects mice from lethal VSV neuropathogenesis. PLoS Pathog. 8:e1002712. doi:10.1371/journal.ppat.1002712.

Citation: Cell Death and Disease (2013) 4, e465; doi:10.1038/cddis.2012.201

www.nature.com/cddis

TNF can activate RIPK3 and cause programmed necrosis in the absence of RIPK1

DM Moujalled[1,2], WD Cook[3], T Okamoto[4], J Murphy[1,2], KE Lawlor[1,2], JE Vince[1,2] and DL Vaux*[,1,2]

Ligation of tumor necrosis factor receptor 1 (TNFR1) can cause cell death by caspase 8 or receptor-interacting protein kinase 1 (RIPK1)- and RIPK3-dependent mechanisms. It has been assumed that because RIPK1 bears a death domain (DD), but RIPK3 does not, RIPK1 is necessary for recruitment of RIPK3 into signaling and death-inducing complexes. To test this assumption, we expressed elevated levels of RIPK3 in murine embryonic fibroblasts (MEFs) from wild-type (WT) and gene-deleted mice, and exposed them to TNF. Neither treatment with TNF nor overexpression of RIPK3 alone caused MEFs to die, but when levels of RIPK3 were increased, addition of TNF killed WT, *Ripk1*$^{-/-}$, *caspase* 8$^{-/-}$, and *Bax*$^{-/-}$/*Bak*$^{-/-}$ MEFs, even in the presence of the broad-spectrum caspase inhibitor Q-VD-OPh. In contrast, *Tnfr1*$^{-/-}$ and *Tradd*$^{-/-}$ MEFs did not die. These results show for the first time that in the absence of RIPK1, TNF can activate RIPK3 to induce cell death both by a caspase 8-dependent mechanism and by a separate Bax/Bak- and caspase-independent mechanism. RIPK1 is therefore not essential for TNF to activate RIPK3 to induce necroptosis nor for the formation of a functional ripoptosome/necrosome.
Cell Death and Disease (2013) 4, 465; doi:10.1038/cddis.2012.201; published online 17 January 2013
Subject Category: Experimental Medicine

By binding to tumor necrosis factor receptor 1 (TNFR1), TNF can activate both transcription factors, such as AP-1 and NF-κB, as well as cell death mechanisms.[1] Because most cell lines are not killed by the addition of TNF alone, but many die when TNF is added together with inhibitors of transcription or translation, such as actinomycin D or cycloheximide (CHX),[2] these transcription factor pathways appear to promote cell survival. Consistent with this notion, cell lines mutant for the p65/RelA component of NF-κB are killed by TNF alone.[3] These observations show that upon ligation, TNFR1 not only activates the NF-κB pathway but also triggers cell death pathways that can be blocked by an NF-κB-dependent process.

TNF activates a number of different death mechanisms depending of the cell type and circumstances. In many cell types, including mouse embryonic fibroblasts (MEFs), cell death triggered by TNF (plus CHX), or by related ligands such as TRAIL or FasL, requires the presence of the adaptor protein Fas-associated death domain (FADD) and the protease caspase 8.[4,5] The receptors for these ligands bear cytoplasmic death domains (DDs) that allow them to bind directly or indirectly to FADD, which in turn binds to the death effector domains of procaspase 8, causing it to activate.[6]

Although cell death triggered by ligation of death receptors can often be blocked by the caspase 8 inhibitor crmA[7,8] or by pancaspase inhibitory compounds such as Q-VD-OPh[9] or z-VAD-FMK,[10] not all cells are protected. For example, murine fibrosarcoma L929 cells were killed more efficiently by TNF in the presence of z-VAD-FMK,[11,12] and z-VAD-FMK did not prevent the death of U937 cells treated with TNF, or HT29 cells treated with TNF plus an inhibitor of apoptosis protein (IAP) antagonist (smac-mimetic).[13] Instead, these cells died displaying a characteristic appearance termed 'necroptosis'.[11]

Necroptosis, or programmed necrosis, refers to a caspase 8-independent death mechanism triggered by the receptor-interacting protein kinase 1 and 3 (RIPK1 and RIPK3).[11,14–18] Necroptosis is thought to be dependent on the enzymatic activity of RIPK1, as suggested by the protection conveyed by the RIPK1 kinase inhibitor necrostatin.[19] Because RIPK1, but not RIPK3, bears a DD that can interact with the TNFR1,[20] it has been suggested that upon binding of TNF, RIPK1 is recruited to TNFR1 either directly via its DD or indirectly by a DD-bearing adaptor, such as TNF receptor-associated death domain (TRADD), to form a complex on the cytoplasmic domain of TNFR1.[21] In cells destined to die, this complex is released from TNFR1, and recruits other proteins, such as FADD and caspase 8 to induce apoptosis, or interacts with RIPK3 to cause necroptosis.[22,23] RIPK1 is thought to have a crucial role in recruiting RIPK3 by binding via their shared RIP homotypic interaction motifs (RHIMs).[22,24,25] Therefore, according to this model, RIPK1 recruitment of RIPK3 is essential for ligated TNFR1 to signal necroptosis.[26,27]

[1]The Walter and Eliza Hall Institute of Medical Research, 1G Royal Parade, Melbourne, Victoria, Australia; [2]Department of Medical Biology, The University of Melbourne, Parkville, Victoria, Australia; [3]Department of Biochemistry, La Trobe Institute for Molecular Science, La Trobe University, Kingsbury Drive Bundoora, Melbourne, Victoria, Australia and [4]Department of Molecular Virology, Research Institute for Microbial Diseases, Osaka University, Yamadaoka, Suita, Osaka, Japan
*Corresponding author: DL Vaux, Department of Biochemistry, La Trobe Institute for Molecular Science, La Trobe University, Kingsbury Drive Bundoora, Melbourne, Victoria 3086, Australia. Tel: +61 3 9345 4129; E-mail: vaux@wehi.edu.au
Keywords: TNF; necroptosis; receptor-interacting protein kinases; smac-mimetic; inhibitor of apoptosis proteins TNF
Abbreviations: CHX, cycloheximide; DD, death domain; TNF, tumor necrosis factor; TNFR1, TNF receptor 1; RIPK1/3, receptor-interacting protein kinases; IAPs, inhibitor of apoptosis proteins; TRADD, TNF receptor-associated death domain; FADD, Fas-associated death domain
Received 28.11.12; accepted 4.12.12; Edited by G Melino

To determine the roles and requirements for TRADD, FADD, caspase 8, RIPK1, RIPK3, and Bax/Bak for TNF-induced cell death, we derived MEFs from gene-deleted mice, and treated them with TNF, in the presence or absence of exogenously expressed RIPK3. We found that addition of TNF activated both caspase 8- and RIPK3-dependent death pathways, even in the absence of RIPK1. Our results show that although TNFR1 and TRADD were necessary for TNF to activate RIPK3 to cause cell death, RIPK1 and FADD were not.

Results

Elevation of RIPK3 allows TNF to cause death of MEFs. To determine whether overexpression of RIPK3 alone was sufficient to cause death of MEFs, we infected wild-type (WT) MEFs with a 4-hydroxytamoxifen (4HT)-inducible lentiviral vector expressing FLAG-tagged RIPK3 (Figure 1a). As expected, in the absence of 4HT, cells treated with TNF for 24 h did not die, whereas those treated with TNF plus a smac-mimetic compound, which depletes cells of cIAP1,[7] did die (Figure 1b, upper panels). Induction of FLAG-RIPK3 by 4HT also failed to kill the cells, but when TNF was added to cells in which FLAG-RIPK3 had been induced, they died (Figure 1b, lower panels). These results show that although elevation of RIPK3 levels alone is not sufficient to cause cell death, it can sensitize MEFs to killing by TNF, even when cIAP1 is present.

TNFR1 and TRADD are required for TNF to cause death of MEFs with elevated RIPK3. TNFR1 signaling involves formation of two distinct signaling complexes, the transient membrane-associated TNFR1 signaling complex (complex I) and the cytoplasmic signaling complex termed complex II.[21] To determine components required for TNF to cause death of cells expressing elevated RIPK3, we tested MEF lines that were mutant for proteins implicated in TNF signaling. We infected *Tnfr1*$^{-/-}$, *Tnfr2*$^{-/-}$, and *Tradd*$^{-/-}$ MEFs with the inducible lentiviral vector expressing FLAG-tagged RIPK3 (Supplementary Figure 1a).

Unlike WT MEFs and those mutant for TNFR2, the *Tnfr1*$^{-/-}$ and *Tradd*$^{-/-}$ MEFs were not killed when RIPK3 expression was induced with 4HT and TNF was added (Figure 2). Therefore, both TNFR1 and TRADD are required for TNF to activate RIPK3's killing function.

TNF can activate RIPK3 and cause cell death in the absence of caspase 8 and RIPK1. Numerous reports have described 'programmed necrosis' or 'necroptosis' as forms of cell death mediated by the serine/threonine kinases RIPK1 and RIPK3 that are independent of caspase 8.[11,14,18] To determine whether TNF-triggered death of cells with elevated RIPK3 required caspase 8, we generated *caspase 8*$^{-/-}$ MEFs by deleting loxP-flanked caspase 8 alleles *in vitro* (Supplementary Figure 1b), and then infected them with the 4HT-inducible RIPK3 lentivirus.

First, we compared the sensitivity of WT, *caspase 8*$^{-/-}$, and *Ripk1*$^{-/-}$ MEFs to killing by TNF plus smac-mimetic (Figure 3a). Unlike WT MEFs, which were efficiently killed by TNF plus smac-mimetic, very few of the *Ripk1*$^{-/-}$ and *caspase 8*$^{-/-}$ cells died, indicating that when IAPs are depleted by smac-mimetic, TNF triggers death of MEFs by a RIPK1- and caspase 8-dependent mechanism.[28,29] This requirement of RIPK1 and caspase 8 for killing of MEFs by TNF plus smac-mimetic is similar to that observed in neuroblastoma cells treated with TRAIL and IAP inhibitor.[30]

To determine whether TNF-triggered death of MEFs with elevated RIPK3 used the same mechanism as when TNF caused death of IAP-depleted cells, we infected the *caspase 8*$^{-/-}$ and *Ripk1*$^{-/-}$ MEFs with the inducible

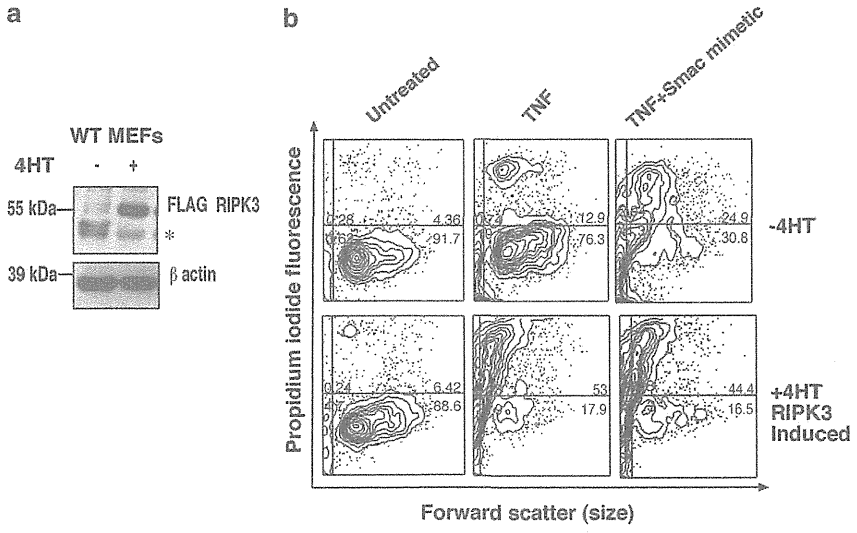

Figure 1 TNF causes death of cells with elevated RIPK3. (**a**) WT MEFs were infected with a lentiviral vector-expressing FLAG RIPK3. Cells were induced with 10 nM 4HT for 24 h, and lysates were probed for FLAG. β-Actin was used as a loading control. *, indicates a nonspecific band. (**b**) Expression of FLAG-RIPK3 in MEFs was induced with 10 nM 4HT for 24 h (lower panels), and cells were then treated with 100 ng/ml TNF or TNF plus 500 nM smac-mimetic for a further 24 h. Cells were stained with PI and analyzed by flow cytometry to detect loss of plasma membrane integrity

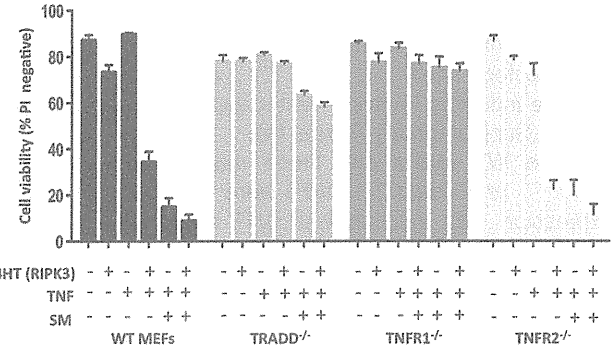

Figure 2 TNFR1 and TRADD are necessary for TNF to cause death of MEFs treated with smac-mimetic or with elevated RIPK3. FLAG-RIPK3 was induced in WT, *Tnfr1*$^{-/-}$, *Tnfr2*$^{-/-}$, and *Tradd*$^{-/-}$ MEFs with 10 nM 4HT for 24 h. Cells were then treated with 100 ng/ml TNF or TNF plus 500 nM smac-mimetic for a further 24 h, stained with PI, and analyzed by flow cytometry. Columns show mean ± S.E.M., where $n = 3$ independently performed experiments

lentiviral vector bearing FLAG-tagged RIPK3 (Figure 3b and Supplementary Figure 1c). When FLAG-RIPK3 was induced in *Ripk1*$^{-/-}$ and *caspase 8*$^{-/-}$ MEFs, little cell death occurred (Figure 3c). There was also little cell death when TNF was added alone. However, addition of TNF to cells in which RIPK3 had been induced by 4HT strongly induced cell death, both in short-term (Figure 3c) and long-term clonogenic survival assays (Figure 3d). Therefore, neither RIPK1 nor caspase 8 is required for TNF to induce cell death when RIPK3 levels are elevated, but both are needed for TNF to kill cells in which IAPs are depleted by a smac-mimetic (Figure 3b). This indicates that while death of MEFs caused by TNF plus smac-mimetic requires both RIPK1 and caspase 8 activity, when RIPK3 levels are elevated, TNF can induce a RIPK1- and caspase 8-independent death mechanism.

RIPK3 killing triggered by TNF does not require Bax/Bak. Although several groups have shown that RIPK1 and RIPK3 can trigger a caspase-independent, necrotic form of cell death, a number of different effector mechanisms have been proposed. For example, it has been reported that in some cells, RIP kinases cause cell death by stimulating production of reactive oxygen species (ROS) or by disrupting mitochondrial integrity.[14] In addition, Zhang *et al.*[18] suggested that RIPK3 generates ROS by interacting with the mitochondrial metabolic enzymes glutamate dehydrogenase and glycogen phosphorylase, whereas another group proposed that RIPK3 induces cell death by interacting with MLKL and PGAM5, and activating DRP-1 to cause mitochondrial dysfunction;[17,22] a fourth group found that binding to DNA-dependent activator of interferon regulatory factors (DAI) was necessary for RIPK3 to cause necrosis;[31] and a fifth group reported that Bax or Bak was necessary for TNF-induced necrosis.[32] To determine whether RIPK3 causes cell death by activating the intrinsic (Bax/Bak-dependent) pathway, we infected *Bax*$^{-/-}$/*Bak*$^{-/-}$ MEFs with an inducible lentiviral vector encoding FLAG RIPK3 (Supplementary Figure 1d), and treated the cells with TNF. As shown in Figure 4, when RIPK3 levels were elevated, TNF caused a similar amount of death of *Bax*$^{-/-}$/*Bak*$^{-/-}$ as of WT MEFs, indicating that activated RIPK3 can kill cells by a Bax/Bak-independent mechanism. Furthermore, as the broad-spectrum caspase inhibitor Q-VD-OPh was not able to prevent death of the *Bax*$^{-/-}$/*Bak*$^{-/-}$ MEFs, RIPK3 must be able to activate a death mechanism that is not only independent of Bax and Bak but also does not require caspase activity.

When RIPK3 levels are elevated, TNF activates caspases whether RIPK1 is present or not. Even though it was clear that when RIPK3 levels were elevated, TNF could trigger cell death by a caspase 8-independent mechanism (Figures 3c and d), TNF is also capable of activating caspase 8, because when IAPs were depleted by smac-mimetic, TNF killed WT, but not *caspase 8*$^{-/-}$ cells (Figures 3c and d). To see whether TNF could activate caspase 8 when RIPK3 levels were elevated, we treated WT and *Ripk1*$^{-/-}$ MEFs with 4HT to induce FLAG-RIPK3, added TNF, and after 4 h lysed the cells and analyzed them by western blot (Figure 5a). Addition of TNF was able to trigger processing of caspase 8, but only when FLAG-RIPK3 was induced. Strikingly, caspase 8 processing was triggered by the addition of TNF both in the WT and *Ripk1*$^{-/-}$ MEFs, indicating that when RIPK3 levels are elevated, TNFR1 can signal via RIPK3 to activate caspase 8 even in the absence of RIPK1.

To further analyze the caspase pathways that were activated by TNF in cells with elevated RIPK3, we performed additional experiments in *Ripk1*$^{-/-}$ and *caspase 8*$^{-/-}$ MEFs, using western blots to test for processing of caspase 3 and cleavage of PARP, and taking cells from duplicate wells to assess their viability by flow cytometry.

As shown in Figure 5b, TNF triggered the processing and activation of caspase 3 and PARP cleavage only in cells with elevated RIPK3. Furthermore, when RIPK3 was elevated, TNF caused activation of caspase 3 in *Ripk1*$^{-/-}$ MEFs, but not in *caspase 8*$^{-/-}$ MEFs.

Taken together, these experiments show that when ligated, TNFR1 can signal to RIPK3 independently of RIPK1, and if its levels are high enough, RIPK3 can activate caspase 8 and caspase 3 even if RIPK1 is absent. Nevertheless, activated caspase 8 was not required for most of the death when TNF was added to cells with elevated RIPK3, because Q-VD-OPh was not able to prevent their death (Figure 5c, WT and *Ripk1*$^{-/-}$ gray columns), and cell death still occurred even in the *caspase 8*$^{-/-}$ MEFs (Figure 5c, light gray columns).

TNF can activate RIPK3 in the absence of FADD. To determine whether FADD was required for TNFR1 to activate RIPK3, we transfected the RIPK3-inducible construct into *Fadd*$^{-/-}$ MEFs. When these cells were treated with 4HT (to induce RIPK3) and TNF, they did not die. However, as western blots showed that the *Fadd*$^{-/-}$ MEFs expressed relatively low levels of MLKL, a protein thought to be necessary for RIPK3-induced cell death,[22,33] we hypothesized that the *Fadd*$^{-/-}$ MEFs might be surviving because of low levels of MLKL, rather than because they lacked FADD. To resolve this, we transfected the *Fadd*$^{-/-}$ cells with a second vector bearing a doxycycline-inducible MLKL construct (Figure 6a). Addition of TNF to *Fadd*$^{-/-}$ cells

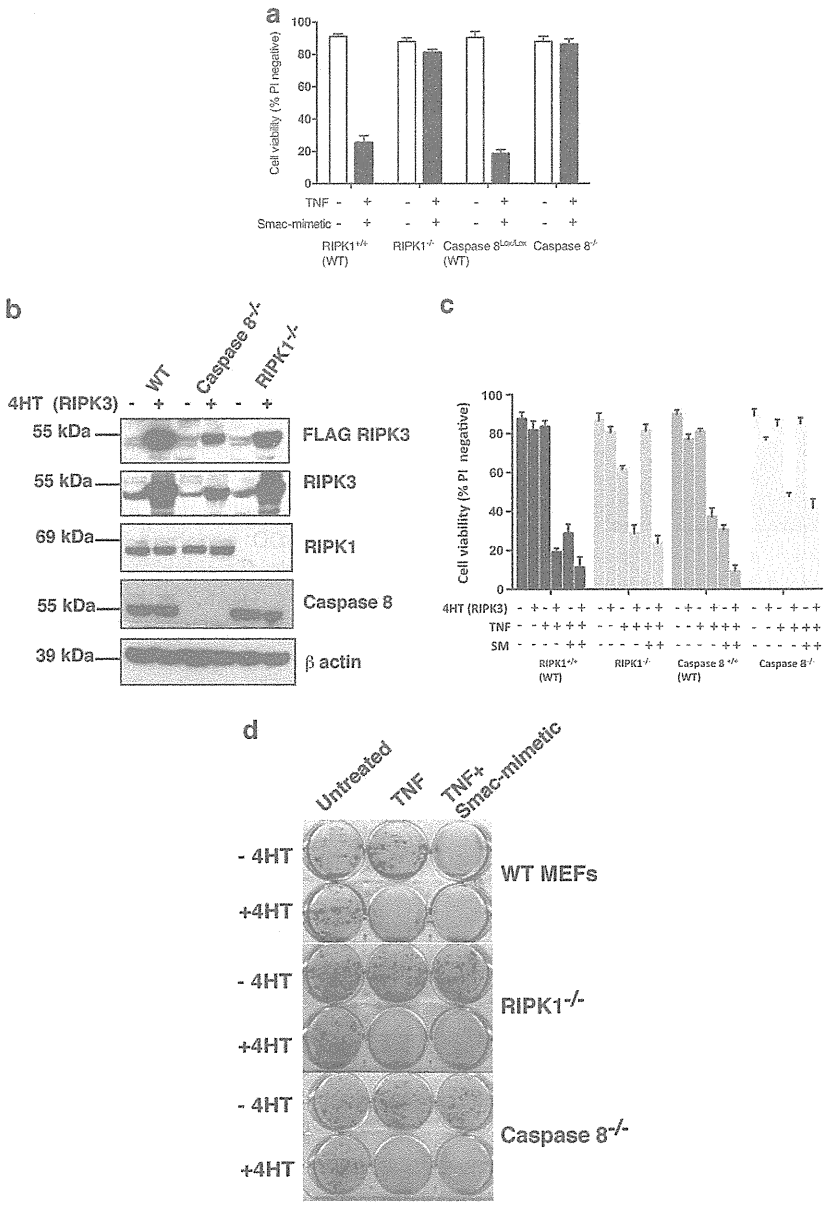

Figure 3 Both caspase 8 and RIPK1 are required for TNF plus smac-mimetic to cause cell death, but when levels of RIPK3 are elevated, TNF alone can induce cell death in the absence of caspase 8 or RIPK1. (**a**) MEF lines were untreated (white bars) or treated with 100 ng/ml TNF plus 500 nM smac-mimetic (black bars) for 24 h. Cell viability was determined by PI exclusion using a flow cytometer. Columns show mean ± S.E.M., where $n = 3$ independently performed experiments. (**b**) WT, *caspase* $8^{-/-}$, and *Ripk1*$^{-/-}$ MEFs bearing the inducible FLAG RIPK3 vector were untreated or treated with 10 nM 4HT for 24 h, and lysates were probed with antibodies to reveal levels of endogenous or induced FLAG-tagged proteins. (**c**) Cell lines were induced with 10 nM 4HT for 24 h, and then treated, where indicated, with 100 ng/ml TNF and 500 nM smac-mimetic (SM) for a further 24 h, and viability determined by flow cytometric analysis of PI exclusion. Columns show mean ± S.E.M., where $n = 3$ independently performed experiments. (**d**) Cell lines were induced with 10 nM 4HT for 24 h and cultured with 100 ng/ml TNF alone or TNF plus 500 nM smac-mimetic for 48 h. Cells were resuspended using trypsin, re-plated, and after 5 days stained with crystal violet to assess clonogenicity

in which both RIPK3 and MLKL were induced increased the amount of cell death (Figure 6b). Therefore, in these cells ligated TNFR1 was able to activate RIPK3 and MLKL in the absence of FADD. Furthermore, we could show upon induction of RIPK3, MLKL, and TNF treatment, there was no caspase 8 cleavage in the *Fadd*$^{-/-}$ MEFs as compared to WT MEFs with RIPK3 overexpression and TNF treatment (Figure 6c). Therefore, in order for RIPK3 to induce activation and cleavage of caspase 8, it requires FADD.

Discussion

We set out to determine the requirements for particular signaling components involved in cell death in response to TNF. To do so, we used MEFs derived from gene-deleted mice. Consistent with many earlier reports, addition of TNF to WT MEFs did not cause them to die,[29,34] but when the cells had been treated with a smac-mimetic compound that depletes cells of cIAP1, addition of TNF did cause cell death.

As TNF plus smac-mimetic did not kill *Ripk1*$^{-/-}$ or *caspase 8*$^{-/-}$ MEFs, which were able to divide and form colonies, cIAP1 in WT MEFs must prevent activation of a TNF-induced death pathway that requires both RIPK1 and caspase 8.

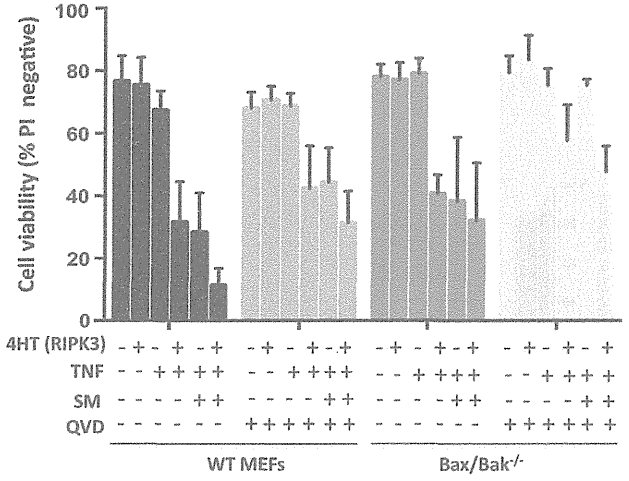

Figure 4 Death induced by TNF and activated RIPK3 is independent of proapoptotic Bcl-2 family proteins Bax and Bak. WT and *Bax*$^{-/-}$/*Bak*$^{-/-}$ MEFs bearing the inducible FLAG-RIPK3 vector were induced with 10 nM 4HT for 24 h. Where indicated, cells were pretreated with 10 μM Q-VD-OPh for 1 h and subsequently treated with 100 ng/ml TNF or TNF plus 500 nM smac-mimetic (SM) for 24 h. Cells were stained with PI and cell viability determined by flow cytometry. Columns show mean ± S.E.M., where $n = 3$ independently performed experiments

Although the MEF lines expressed endogenous RIPK3, to determine if overexpression of RIPK3 alone was sufficient to induce necroptosis, we expressed additional RIPK3 from an inducible lentiviral vector. Overexpression of RIPK3 alone was not sufficient to cause death of MEFs, but unlike WT cells, cells with increased RIPK3 died upon addition of TNF. We found that when RIPK3 levels were increased, TNF triggered activation of caspase 8, whether RIPK1 was present or not. These results show that when ligated, TNFR1 can activate RIPK3, and thereby cause activation of caspases 8 and 3, cleavage of PARP, and cell death, even when RIPK1 was absent.

These findings question prior assumptions that because it bears a DD, RIPK1 was essential for TNF to induce activation of RIPK3, or was essential for TNF to activate caspase 8. Although we do not know precisely how TNFR1 activates RIPK3 in the absence of RIPK1, TRADD appears to be necessary, but to date there have been no reports showing that TRADD can bind to RIPK3. TRAF2 might also be responsible for recruiting RIPK3 into death-inducing complexes, as TRAF2 is rapidly recruited to complex I upon ligation of TNFR1, and RIPK3 has been reported to co-immunopreciptitate with TRAF2.[35]

We initially wondered if FADD might be responsible for recruiting RIPK3 to death-inducing complexes in the *Ripk1*$^{-/-}$ MEFs, firstly because some preliminary experiments suggested that *Fadd*$^{-/-}$ MEFs did not die when RIPK3 was elevated and cells were treated with TNF, and secondly because it has been reported that FADD can interact directly with RIPK3.[14,23] However, the *Fadd*$^{-/-}$ line had relatively low

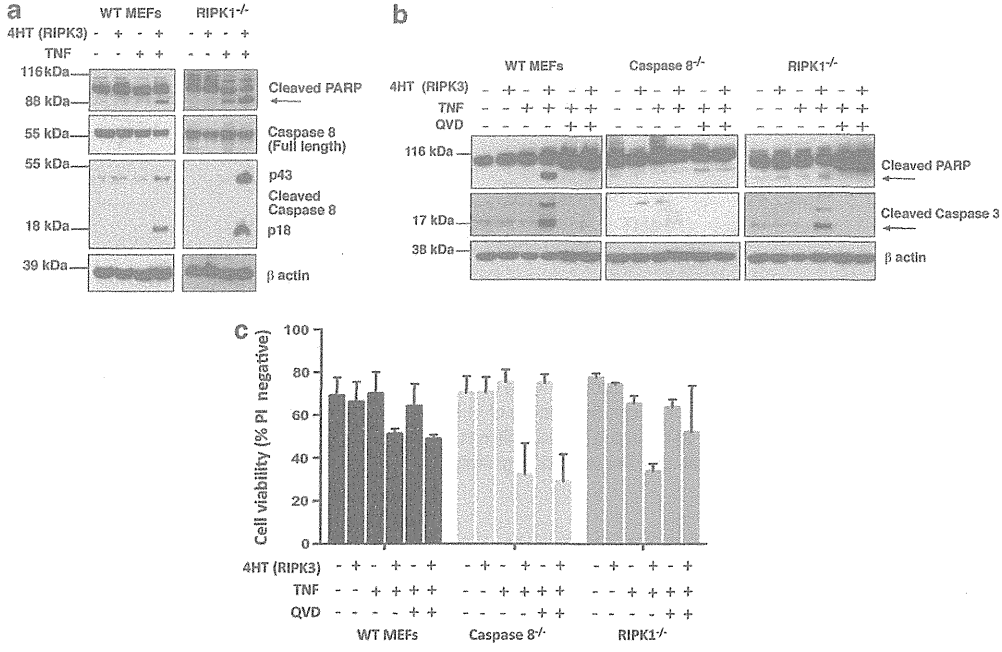

Figure 5 TNF treatment of cells overexpressing RIPK3 activates caspases, but this is not necessary for cell death. (**a**) WT and *Ripk1*$^{-/-}$ MEFs were induced with 10 nM 4HT for 24 h and treated with 100 ng/ml TNF. After 4 h, cells were harvested, lysed, and analyzed by western blotting, and probed for poly (ADP-ribose) polymerase (PARP) and both full-length and cleaved caspase 8. β-Actin was used as a loading control. (**b**, **c**) WT (*caspase 8*$^{lox/lox}$), *caspase 8*$^{-/-}$, and *Ripk1*$^{-/-}$ MEFs in duplicate wells were induced with 10 nM 4HT for 24 h and treated with 100 ng/ml TNF. (**b**) After 4 h, cells from one set of wells were harvested, lysed, and analyzed by western blot probed for PARP and cleaved caspase 3. (**c**) After 4 h in culture, the cells in the second set of wells were re-suspended, stained with 100 ng/ml PI, and cell viability determined by flow cytometry. Columns show mean ± S.E.M., where $n = 3$ independently performed experiments

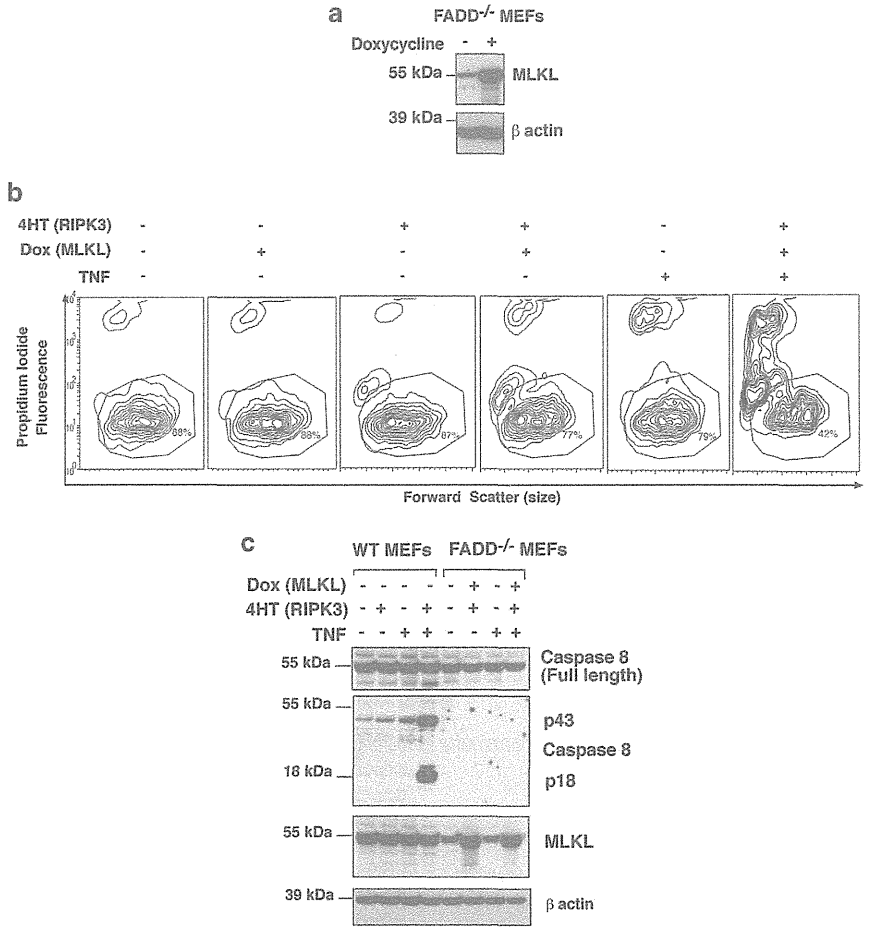

Figure 6 Elevated levels of MLKL in *Fadd*$^{-/-}$ MEFs allows cell death by TNF-induced activation of RIPK3. (**a**) *Fadd*$^{-/-}$ MEFs were infected with a doxycycline (dox)-inducible MLKL expression vector. Cells were treated with 1 μg/ml of dox for 24 h. Cell lysates were harvested and probed for MLKL as indicated and β-actin was used as a loading control. (**b**) *Fadd*$^{-/-}$ MEFs bearing vectors for dox-inducible MLKL and 4HT-inducible RIPK3 were treated with 1 μg/ml dox, 10 nM 4HT, and 100 ng/ml TNF for 24 h. Cells were re-suspended using trypsin, stained with 100 ng/ml PI, and analyzed by flow cytometry. (**c**) WT MEFs bearing a 4HT-inducible RIPK3 vector and *Fadd*$^{-/-}$ MEFs bearing vectors for 4HT-inducible RIPK3 and dox-inducible MLKL were treated with 1 μg/ml dox and 10 nM 4HT for 24 h and treated with 100 ng/ml TNF for 4 h. Cell lysates were harvested and probed for caspase 8 (full-length), cleaved caspase 8 and MLKL as indicated, and β-actin was used as a loading control

levels of MLKL, and when MLKL levels were elevated, TNF was able to kill the *Fadd*$^{-/-}$ cells. These results suggest that FADD might be needed for activation of caspase 8, but is not required for TNFR1 to activate RIPK3 and MLKL to cause necroptosis.

The necroptotic cell death pathway triggered by TNF in cells with elevated RIPK3 did not require the presence of FADD, RIPK1, caspase 8, or Bax/Bak. The ability of induced MLKL to restore the sensitivity of the *Fadd*$^{-/-}$ cells is consistent with MLKL being activated by RIPK3 and having an important role in necroptosis.[22] Although how MLKL kills has not yet been determined with certainty, our observations are consistent with reports that it causes cell death by a caspase- and Bax/Bak-independent mechanism.[17,22]

Our results are consistent with the model shown in Figure 7. WT MEFs remain viable when TNF is added, because cIAP1, TRAF2, and RIPK1 allow activation of canonical NF-κB pathways resulting in the expression of cell death inhibitors such as FLIP, cIAP2, and A20[28,36,37] (panel 1). When smac-mimetic is added, it causes autoubiquitylation and degradation of IAPs, so that cells treated with TNF plus smac-mimetic die by a caspase 8- and RIPK1-dependent mechanism (panel 2).

When levels of RIPK3 are elevated (panel 3), ligation of TNFR1 signals via TRADD to activate RIPK3, and TNF can trigger RIPK3 activation even when RIPK1 is absent. Once activated, RIPK3 can in turn activate two distinct cell death pathways, one involving caspase 8, and another that involves MLKL (panel 3). In *Fadd*$^{-/-}$ MEFs, ligation of TNFR1 can activate RIPK3 when its levels are elevated, and it can activate the necroptotic pathway but not the caspase 8-dependent cell death pathway (panel 4).

These findings do not exclude the possibility that RIPK1 can activate RIPK3; indeed, this is likely to be what occurs when necrostatin is able to inhibit cell death.[11,19] These findings are also consistent with a model in which RIPK1 acts in parallel with RIPK3 such that in the presence of RIPK1, lower levels of RIPK3 are needed for necroptosis. However, our results provide strong evidence that RIPK1 does not have an obligatory role in necroptosis signaling, challenging models

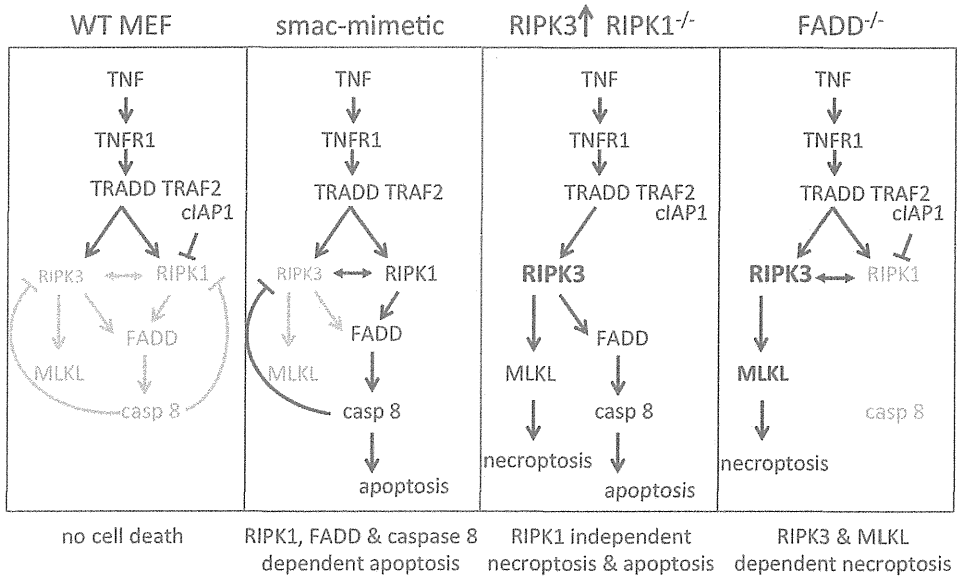

Figure 7 Model for activation of caspase-dependent and -independent cell death mechanisms by TNF. Under normal conditions, TNF treatment of WT MEFs does not induce cell death. When IAPs are depleted with smac-mimetic, TNF can activate caspase 8 by a pathway requiring RIPK1 to cause cell death that can be blocked by the caspase inhibitor Q-VD-OPh. When levels of RIPK3 are elevated, TNF not only activates caspase 8 but also activates a caspase-independent death mechanism, but it does not require RIPK1 for either

which suggested that RIPK1 has an essential role upstream of RIPK3 and is required for its activation.

Materials and Methods

Genetically modified cell lines and mice. Production of MEF lines has been described previously in detail.[7] Briefly, primary MEFs were generated from E15.5 embryos and then infected with SV40 large T antigen-expressing lentivirus to generate immortal cell lines. *Ripk1*$^{-/-}$ mice were provided by Michelle Kelliher (University of Massachusetts Medical School, Worcester, MA, USA) and *Tnfr1*$^{-/-}$ and *Tnfr2*$^{-/-}$ mice were a kind gift from Heinrich Korner (University of Tasmania, Sandy Bay, TAS, Australia). *Fadd*$^{-/-}$ MEFs were provided by Francis Chan (University of Massachusetts Medical School), *Tradd*$^{-/-}$ MEFs were obtained from Henning Walczak (Imperial College, London, UK) and Manolis Pasparakis (University of Cologne, Cologne, Germany), and *Bax/Bak*$^{-/-}$ MEFs were provided by David Huang (Walter and Eliza Hall Institute, Parkville, VIC, Australia). Caspase 8 conditional knockin mice were provided by Stephen Hedrick (University of California San Diego, San Diego, CA, USA).

Generation of *caspase 8*$^{-/-}$ MEFs. Caspase 8 gene-deleted MEFs were generated from E8.5 caspase 8 LoxP/LoxP embryos (Dr. Steve Hedrick, University of California San Diego). Primary MEFs were immortalized by infection with SV40 largeT antigen-expressing lentivirus as described previously.[7] To delete caspase 8, the transformed MEFs were infected with a Cre-recombinase-expressing lentivirus (pFU CreR SV40 Hygro) and deletion was confirmed by western blot.

Cell culture, transfections, constructs and lentiviral infections. Cell lines were maintained at 37° C, 10% CO_2 in DMEM supplemented with 10% (v/v) fetal bovine serum (Gibco, Melbourne, VIC, Australia), 50 μg/ml penicillin G, 50 U/ml streptomycin, and 2 mM L-glutamine. Medium for *Bax/Bak*$^{-/-}$ MEFs was also supplemented with 270 μM L-asparagine and 50 μM 2-mercaptoethanol. Cre-recombinase and SV40 large T antigen were cloned into the lentiviral vector pFU as described previously.[7] Mouse FLAG-RIPK3 was cloned into the 4HT-inducible lentiviral vector pF 5× UAS.[7,38] Lentiviruses were generated by transfecting subconfluent 10 cm plates of 293T cells with vector plasmids together with the packaging constructs pCMV-ΔR8 and pVSV-G using Effectene (Qiagen, Chadstone, VIC, Australia) as described previously.[38] After 48 h, viral supernatants were collected, filtered, supplemented with 4 μg/ml polybrene, and added to the target MEFs. Stably infected cells were selected in the presence of 5 μg/ml puromycin (puro) and 300 μg/ml hygromycin B. Expression of pF 5× UAS-inducible constructs was induced with 10 nM 4HT, unless otherwise indicated. The doxycycline-inducible vector pF TRE3G PGK puro is a derivative of the pRetroX retroviral vector (Clontech, Mountain View, CA, USA) possessing a Tet-On 3G transactivator (Tet3G), a puro resistance gene expressed under the control of a PGK promoter, and a tetracycline-responsive element.[39] The cDNA-encoding mouse MLKL (residues 1–464; UniProt sequence Q9D2Y4-2) was PCR amplified using the following primers: forward, 5′-CGCGGATCCAAGCCACCATGGCGCGC CAGGAC-3′; reverse, 5′-CGCGGATCCTTACACCTTCTTGTCCGTGGATTC-3′. The *Bam*HI-digested PCR product was ligated into the *Bam*HI site of the pF TRE3G PGK puro vector and was verified by sequencing (Micromon DNA Sequencing Facility, Clayton, VIC, Australia).

Antibodies and chemicals. Primary antibodies used for western blot analysis were anti-FLAG (F-3165; Sigma, Croydon, VIC, Australia), anti-β-actin (A-1978; Sigma), anti-RIPK1 (610458; BD Transduction Laboratories, North Ryde, NSW, Australia), anti-RIPK3 (551042; Pharmingen, North Ryde, NSW, Australia), anticaspase 8 (Lorraine O'Reilly, The Walter and Eliza Hall Institute, Melbourne, VIC, Australia), anticleaved caspase 8 (Asp 387) (8592; Cell Signaling Technology, Arundel, QLD, Australia), anticleaved caspase 3 (Asp 175) (9661; Cell Signaling Technology), anti-PARP (9542; Cell Signaling Technology, Arundel, Queensland Australia), and anti-MLKL (Jian-Guo Zhang, The Walter and Eliza Hall Institute). 4HT and doxycycline were purchased from Sigma, Fc-TNF (in-house) and Q-VD-OPh (OPH001) from SM Biochemicals, (Anaheim, CA, USA) and smac-mimetic was obtained from TetraLogic Pharmaceuticals (Malvern, PA, USA).

Cell death assays. Cells were seeded at approximately 40% confluency onto 12-well tissue culture plates and were allowed to settle for 16–20 h. Where indicated, 500 nM smac-mimetic (Compound A; TetraLogic Pharmaceuticals), 100 ng/ml human Fc-TNF, 10 nM 4HT, and/or 10 μM Q-VD-OPh were added to cells for 24 h and cell death measured by uptake of propidium iodide (PI) using a FACScalibur flow cytometer (BD Biosciences, North Ryde, NSW, Australia). In all, 10 000 events per sample were collected, and the percentage of live cells (% PI-negative cells) was quantified using WEASEL software (version 2.2.2; WEHI).

Clonogenic survival assay. WT, *caspase 8*$^{-/-}$, *Ripk1*$^{-/-}$, and *Bax/Bak*$^{-/-}$ MEFs were plated at equal densities on six-well plates, and cultured with or without TNF and smac-mimetic for 24 h. After treatment, cells were treated with trypsin, re-suspended, washed, and re-plated. Cells were then grown

for 5 days and fixed with glutaraldehyde, and colonies stained with 0.1% (w/v) crystal violet.

Western blotting. Lysates were prepared in DISC lysis buffer (20 mM Tris-HCl (pH 7.4), 150 mM NaCl, 10% glycerol, 10% Triton X-100), supplemented with protease inhibitor cocktail (Roche, Dee Why,NSW Australia). Protein samples were separated on 4–12% polyacrylamide gels (Invitrogen, Mulgrave, VIC, Australia), and transferred to Hybond C nitrocellulose membrane (GE, Rydalmere, NSW, Australia) for incubation with specified antibodies. All membrane blocking steps and antibody dilutions were performed using 5% (v/v) skim milk in PBS containing 0.1% (v/v) Tween-20 phosphate-buffered saline (PBST), and washing steps performed with PBST. Western blots were visualized by enhanced chemiluminescence (GE).

Conflict of Interest

The authors declare no conflict of interest.

Acknowledgements. *This work was funded by NHMRC grants and fellowships 433063, 461221, 541901, 575512, 637342, 1003435, and ARC fellowship FT100100100, and was made possible through Victorian State Government Operational Infrastructure Support and Australian Government NHMRC IRIISS. We thank Stephen Hedrick, Michelle Kelliher, and Heinrich Korner for caspase 8, TRADD, FADD, and RIPK1 gene-deleted cell lines and mice, and Mark McKinlay (TetraLogic Pharmaceuticals) for smac-mimetic compound. We would also like to acknowledge Ian Gentle for helping construct the 4HT-inducible FLAG RIPK3 construct.*

1. Baud V, Karin M. Signal transduction by tumor necrosis factor and its relatives. *Trends Cell Biol* 2001; **11**: 372–377.
2. Laster SM, Wood JG, Gooding LR. Tumor necrosis factor can induce both apoptic and necrotic forms of cell lysis. *J Immunol* 1988; **141**: 2629–2634.
3. Beg AA, Baltimore D. An essential role for Nf-Kappa-B in preventing Tnf-alpha-induced cell death. *Science* 1996; **274**: 782–784.
4. Chinnaiyan AM, Tepper CG, Seldin MF, Orourke K, Kischkel FC, Hellbardt S *et al.* Fadd/mort1 is a common mediator of cd95 (fas/apo-1) and tumor necrosis factor receptor-induced apoptosis. *J Biol Chem* 1996; **271**: 4961–4965.
5. Varfolomeev EE, Boldin MP, Goncharov TM, Wallach D. A potential mechanism of cross-talk between the p55 tumor necrosis factor receptor and fas/apo1 – proteins binding to the death domains of the two receptors also bind to each other. *J Exp Med* 1996; **183**: 1271–1275.
6. Muzio M, Stockwell BR, Stennicke HR, Salvesen GS, Dixit VM. An induced proximity model for caspase-8 activation. *J Biol Chem* 1998; **273**: 2926–2930.
7. Vince JE, Wong WW, Khan N, Feltham R, Chau D, Ahmed AU *et al.* IAP antagonists target cIAP1 to induce TNFalpha-dependent apoptosis. *Cell* 2007; **131**: 682–693.
8. Zhou Q, Snipas S, Orth K, Muzio M, Dixit VM, Salvesen GS. Target protease specificity of the viral serpin crma – analysis of five caspases. *J Biol Chem* 1997; **272**: 7797–7800.
9. Caserta TM, Smith AN, Gultice AD, Reedy MA, Brown TL. Q-VD-OPh a broad spectrum caspase inhibitor with potent antiapoptotic properties. *Apoptosis* 2003; **8**: 345–352.
10. Kunstle G, Leist M, Uhlig S, Revesz L, Feifel R, Mackenzie A *et al.* Ice-protease inhibitors block murine liver injury and apoptosis caused by cd95 or by tnf-alpha. *Immunol Lett* 1997; **55**: 5–10.
11. Degterev A, Huang Z, Boyce M, Li Y, Jagtap P, Mizushima N *et al.* Chemical inhibitor of nonapoptotic cell death with therapeutic potential for ischemic brain in jury. *Nat Chem Biol* 2005; **1**: 112–119.
12. Vercammen D, Beyaert R, Denecker G, Goossens V, Van Loo G, Declercq W *et al.* Inhibition of caspases increases the sensitivity of L929 cells to necrosis mediated by tumor necrosis factor. *J Exp Med* 1998; **187**: 1477–1485.
13. Declercq W, Vanden Berghe T, Vandenabeele P. RIP kinases at the crossroads of cell death and survival. *Cell* 2009; **138**: 229–232.
14. Cho YS, Challa S, Moquin D, Genga R, Ray TD, Guildford M *et al.* Phosphorylation-driven assembly of the RIP1–RIP3 complex regulates programmed necrosis and virus-induced inflammation. *Cell* 2009; **137**: 1112–1123.
15. Feoktistova M, Geserick P, Kellert B, Dimitrova DP, Langlais C, Hupe M *et al.* cIAPs block ripoptosome formation, a RIP1/caspase-8 containing intracellular cell death complex differentially regulated by cFLIP isoforms. *Mol Cell* 2011; **43**: 449–463.
16. Tenev T, Bianchi K, Darding M, Broemer M, Langlais C, Wallberg F *et al.* The ripoptosome, a signaling platform that assembles in response to genotoxic stress and loss of IAPs. *Mol Cell* 2011; **43**: 432–448.
17. Wang Z, Jiang H, Chen S, Du F, Wang X. The mitochondrial phosphatase PGAM5 functions at the convergence point of multiple necrotic death pathways. *Cell* 2012; **148**: 228–243.
18. Zhang DW, Shao J, Lin J, Zhang N, Lu BJ, Lin SC *et al.* RIP3, an energy metabolism regulator that switches TNF-induced cell death from apoptosis to necrosis. *Science* 2009; **325**: 332–336.
19. Degterev A, Hitomi J, Germscheid M, Ch'en IL, Korkina O, Teng X *et al.* Identification of RIP1 kinase as a specific cellular target of necrostatins. *Nat Chem Biol* 2008; **4**: 313–321.
20. Sun X, Lee J, Navas T, Baldwin DT, Stewart TA, Dixit VM. RIP3 a novel apoptosis-inducing kinase. *J Biol Chem* 1999; **274**: 16871–16875.
21. Micheau O, Tschopp J. Induction of TNF receptor I-mediated apoptosis via two sequential signaling complexes. *Cell* 2003; **114**: 181–190.
22. Sun L, Wang H, Wang Z, He S, Chen S, Liao D *et al.* Mixed lineage kinase domain-like protein mediates necrosis signaling downstream of RIP3 kinase. *Cell* 2012; **148**: 213–227.
23. Vanlangenakker N, Vanden Berghe T, Bogaert P, Laukens B, Zobel K, Deshayes K *et al.* cIAP1 and TAK1 protect cells from TNF-induced necrosis by preventing RIP1/RIP3-dependent reactive oxygen species production. *Cell Death Differ* 2011; **18**: 656–665.
24. He S, Wang L, Miao L, Wang T, Du F, Zhao L *et al.* Receptor interacting protein kinase-3 determines cellular necrotic response to TNF-alpha. *Cell* 2009; **137**: 1100–1111.
25. Kaiser WJ, Offermann MK. Apoptosis induced by the toll-like receptor adaptor TRIF is dependent on its receptor interacting protein homotypic interaction motif. *J Immunol* 2005; **174**: 4942–4952.
26. Li J, McQuade T, Siemer AB, Napetschnig J, Moriwaki K, Hsiao YS *et al.* The RIP1/RIP3 necrosome forms a functional amyloid signaling complex required for programmed necrosis. *Cell* 2012; **150**: 339–350.
27. Vandenabeele P, Declercq W, Van Herreweghe F, Vanden Berghe T. The role of the kinases RIP1 and RIP3 in TNF-induced necrosis. *Sci Signal* 2010; **3**: 4.
28. Moujalled DM, Cook WD, Lluis JM, Khan NR, Ahmed AU, Callus BA *et al.* In mouse embryonic fibroblasts, neither caspase-8 nor cellular FLICE-inhibitory protein (FLIP) is necessary for TNF to activate NF-kappaB, but caspase-8 is required for TNF to cause cell death, and induction of FLIP by NF-kappaB is required to prevent it. *Cell Death Differ* 2011; **5**: 808–815.
29. Wong WW, Gentle IE, Nachbur U, Anderton H, Vaux DL, Silke J. RIPK1 is not essential for TNFR1-induced activation of NF-kappaB. *Cell Death Differ* 2009; **3**: 482–487.
30. Abhari BA, Cristofanon S, Kappler R, von Schweinitz D, Humphreys R, Fulda S. RIP1 is required for IAP inhibitor-mediated sensitization for TRAIL-induced apoptosis via a RIP1/FADD/caspase-8 cell death complex. *Oncogene* 2012; e-pub ahead of print, 13 August 2012; doi:10.1038/onc.2012.337.
31. Upton JW, Kaiser WJ, Mocarski ES. DAI/ZBP1/DLM-1 complexes with RIP3 to mediate virus-induced programmed necrosis that is targeted by murine cytomegalovirus vIRA. *Cell Host Microbe* 2012; **11**: 290–297.
32. Irrinki KM, Mallilankaraman K, Thapa RJ, Chandramoorthy HC, Smith FJ, Jog NR *et al.* Requirement of FADD, NEMO, and BAX/BAK for aberrant mitochondrial function in tumor necrosis factor alpha-induced necrosis. *Mol Cell Biol* 2011; **31**: 3745–3758.
33. Zhao J, Jitkaew S, Cai Z, Choksi S, Li Q, Luo J *et al.* Mixed lineage kinase domain-like is a key receptor interacting protein 3 downstream component of TNF-induced necrosis. *Proc Natl Acad Sci USA* 2012; **109**: 5322–5327.
34. Gentle IE, Wong WW, Evans JM, Bankovacki A, Cook WD, Khan NR *et al.* In TNF-stimulated cells, RIPK1 promotes cell survival by stabilizing TRAF2 and cIAP1, which limits induction of non-canonical NF-kappaB and activation of caspase-8. *J Biol Chem* 2011; **286**: 13282–13291.
35. Yu PW, Huang BC, Shen M, Quast J, Chan E, Xu X *et al.* Identification of RIP3, a RIP-like kinase that activates apoptosis and NFkappaB. *Curr Biol* 1999; **9**: 539–542.
36. Chu ZL, Mckinsey TA, Liu L, Gentry JJ, Malim MH, Ballard DW. Suppression of tumor necrosis factor-induced cell death by inhibitor of apoptosis c-iap2 is under nf-kappa-b control. *Proc Natl Acad Sci USA* 1997; **94**: 10057–10062.
37. He KL, Ting AT. A20 inhibits tumor necrosis factor (TNF) alpha-induced apoptosis by disrupting recruitment of TRADD and RIP to the TNF receptor I complex in Jurkat T cells. *Mol Cell Biol* 2002; **22**: 6034–6045.
38. Callus BA, Moujallad DM, Silke J, Gerl R, Jabbour AM, Ekert PG *et al.* Triggering of apoptosis by Puma is determined by the threshold set by prosurvival Bcl-2 family proteins. *J Mol Biol* 2008; **384**: 313–323.
39. Yamamoto M, Okuyama M, Ma JS, Kimura T, Kamiyama N, Saiga H *et al.* A cluster of interferon-gamma-inducible p65 GTPases plays a critical role in host defense against *Toxoplasma gondii*. *Immunity* 2012; **37**: 302–313.

Supplementary Information accompanies the paper on Cell Death and Disease website (http://www.nature.com/cddis)

ACS chemical biology

Letters

pubs.acs.org/acschemicalbiology

Stabilizing the Pro-Apoptotic BimBH3 Helix (BimSAHB) Does Not Necessarily Enhance Affinity or Biological Activity

Toru Okamoto,[†,‡] Kerry Zobel,[§] Anna Fedorova,[§] Clifford Quan,[§] Hong Yang,[†,‡] Wayne J. Fairbrother,[§] David C. S. Huang,[†,‡] Brian J. Smith,[*,†,‡,∥] Kurt Deshayes,[*,§] and Peter E. Czabotar[*,†,‡]

[†]The Walter and Eliza Hall Institute of Medical Research, 1G Royal Parade, Parkville, Victoria 3052, Australia

[‡]Department of Medical Biology, University of Melbourne, Parkville, Victoria 3010, Australia

[§]Departments of Early Discovery Biochemistry and Protein Engineering, Genentech Inc., 1 DNA Way, South San Francisco, California 94080, United States

[∥]Department of Chemistry, La Trobe Institute for Molecular Sciences, La Trobe University, Melbourne, Victoria 3086, Australia

Supporting Information

ABSTRACT: An attractive approach for developing therapeutic peptides is to enhance binding to their targets by stabilizing their α-helical conformation, for example, stabilized BimBH3 peptides (BimSAHB) designed to induce apoptosis. Unexpectedly, we found that such modified peptides have *reduced* affinity for their targets, the pro-survival Bcl-2 proteins. We attribute this loss in affinity to disruption of a network of stabilizing intramolecular interactions present in the bound state of the native peptide. Altering this network may compromise binding affinity, as in the case of the BimBH3 stapled peptide studied here. Moreover, cells exposed to these peptides do not readily undergo apoptosis, strongly indicating that BimSAHB is not inherently cell permeable.

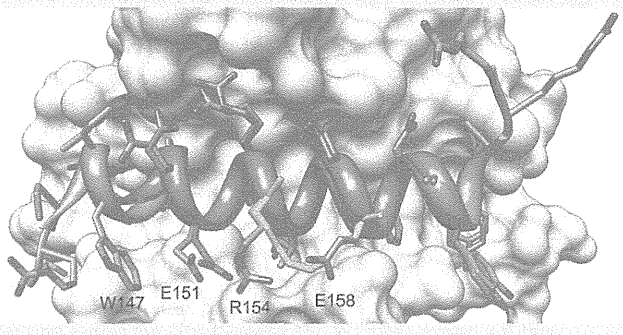

Stabilized helical peptides are designed to mimic an α-helical structure through a constraint imposed by covalently linking two residues on the same helical face (e.g., residue *i* with *i* + 4). "Stapling" the peptide into a preformed helix might be expected to lower the energy barrier for binding by reducing entropic costs, with a concomitant increase in binding affinity. Additionally, stabilizing the peptide may reduce degradation by proteases[1,2] and, in the case of hydrocarbon linkages, reportedly enhance transport into cells,[3] thereby improving bioavailability and their potential as therapeutic agents.[3−5] The findings we present here for the stapled BH3 peptide (BimSAHB), however, do not support these claims, particularly in regards to affinity and cell permeability. We observe a reduction in binding upon BimBH3 stapling, which we attribute to the loss of a network of stabilizing intramolecular interactions on the peptide. Thus, in addition to the primary consideration for staple placement in peptide design, that of avoiding key binding interfaces, our observations reveal a new consideration, that staples should also avoid disruption of favorable interactions within the peptide itself.

It has previously been reported that a stapled version of the BimBH3 peptide (dubbed: "stabilized α-helices of Bcl-2 domains", BimSAHB), where two native residues were replaced with (*S*)-pentenyl alanine derivatives and covalently joined through a metathesis reaction,[2,3] kills cells by directly activating Bax through an interface involving residue Lys21.[6] This stabilized peptide has also been reported to have enhanced binding for the pro-survival proteins.[7] When mouse embryonic fibroblasts (MEFs) (Supplementary Figure 1) or Jurkat cells (data not shown) were treated with BimSAHB, we observed no cell death, in contrast to the potent killing induced by the well-characterized activator of apoptosis, etoposide. This was true for both the 20-mer BimSAHB peptide used below and the 21-mer BimSAHB peptide previously used in cellular assays.[8]

Given that no cell killing was observed when BimSAHB was added to cells in culture, we decided to test the ability of these peptides to induce mitochondrial cytochrome *c* release *in vitro* from cells permeabilized with a low concentration of the detergent digitonin. This would determine if the absence of killing activity could be attributed to a lack of cellular uptake. In such assays, we found that BimSAHB was indeed capable of liberating mitochondrial cytochrome *c* (Figure 1a,b), consistent with the conclusion that BimSAHB, under the conditions tested, does not readily enter cells in sufficient amounts to induce apoptosis (although proteolytic degradation or non-specific binding effects could also account for this observation).

We next tested the role of the Bax interface encompassing Lys21 proposed to be essential for its activation.[6] To undertake

Received: October 18, 2011
Accepted: November 14, 2012

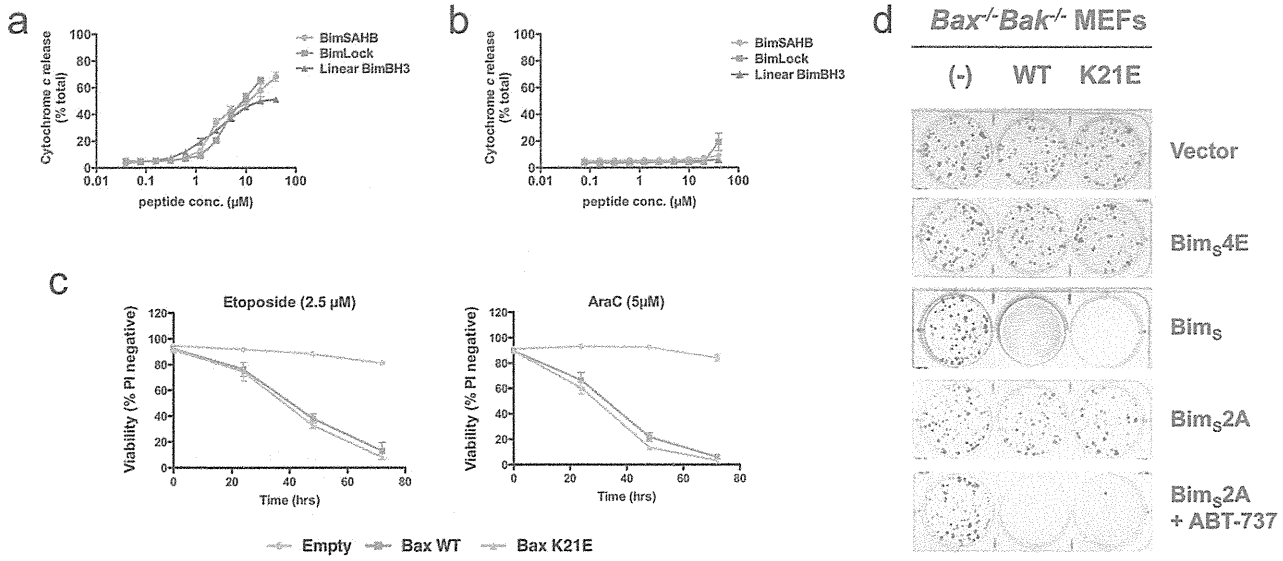

Figure 1. Bioactivity of constrained BimBH3 peptides. Cytochrome *c* release experiments were performed on permeabilized cells (MEFs) that were derived from either (a) wild-type or (b) from $Bax^{-/-}Bak^{-/-}$ mice. The cell pellets, containing intact mitochondria, were treated with increasing concentrations of the indicated peptides. The quantity of cytochrome *c* release was assessed by ELISA (R&D Systems) analyses of supernatants postpeptide treatment as compared to mitochondria treated with the permeabilizing agent 1% Triton X-100 (100% activity). (c) Killing assay of $Bax^{-/-}Bak^{-/-}$ MEF cells reconstituted with either wild-type Bax (WT) or Bax(K21E) in response to DNA damaging agents etoposide or Ara-C. Cell viability was monitored by propidium iodide (PI) exclusion determined by flow cytometry. Expression of wild-type Bax and BaxK21E were confirmed by Western blot analysis (Supplementary Figure 2). (d) Colony formation assays of $Bax^{-/-}Bak^{-/-}$ MEF cells reconstituted with either wild-type Bax (WT) or Bax (K21E) and transfected with vector encoding an inactive Bim variant (Bim$_S$4E),[20] wild-type Bim$_S$ (targeting all pro-survival proteins), a Bim$_S$ variant targeting only Mcl-1 (Bim$_S$2A),[21] or Bim$_S$2A in combination with ABT-737 treatment. Error bars in panels a–c represent SEM of 2 independent experiments.

this, we reconstituted MEFs lacking the essential cell death mediators Bax and Bak with wild-type (WT) Bax or the K21E mutant that was reported to be inert.[6] Unexpectedly, cells reconstituted with either WT or K21E mutant Bax behaved identically in short- or long-term survival assays (Figure 1c,d), suggesting that this interface was not required for Bax activation. Equivalent cell death to that observed for BimBH3 overexpression was observed when ABT-737 (to target Bcl-2, Bcl-x_L, and Bcl-w[7]) was combined with Bim$_S$2A (to target Mcl-1[9]), suggesting that apoptosis in these cells is primarily the result of inhibition of pro-survival proteins (Figure 1d).[10] By implication, the mechanism by which BimBH3 peptides initiate cytochrome *c* release in our experiments using isolated mitochondria could be accounted for by relieving the pro-survival proteins restraining Bax and Bak[10] and possibly by direct activation of Bax via an alternative interface such as that shown for Bak.[11]

In sharp contrast to the reported studies,[3] our studies suggest that BimSAHB is not inherently cell permeable. Moreover, the linear control BimBH3 of precisely the same length as the stapled peptide was just as active at inducing cytochrome *c* release *in vitro* (Figure 1a). As the proposed interface for Bax activation by BimSAHB did not appear to play a major role (Figure 1c,d), we undertook a detailed biochemical and structural analysis of the constrained BimSAHB and its interactions with pro-survival proteins. To undertake these studies, we also employed a second approach, which we termed BimLOCK, to link the side-chains of a glutamate with a lysine through a lactam bridge.[12,13] These modified residues were identical to the (*S*)-pentenyl alanines used to construct BimSAHB.

Circular dichroism (CD) was employed to confirm that covalent linkages enhanced helical content (Figure 2a). Both BimSAHB (39% helix) and BimLOCK (49%) displayed enhanced helical content in an aqueous solution compared to an equivalent linear peptide (21%). Additionally, we determined crystal structures for both constrained peptides in complex with the pro-survival Bcl-2 family protein Bcl-x_L (BCL2L1) (Figure 2b,c). These structures revealed that both constrained peptides bind to Bcl-x_L analogously to the linear BimBH3 peptide and that neither the hydrocarbon staple nor the lactam bridge interacts with residues on Bcl-x_L. Because of the increased helicity, we anticipated an approximate 4-fold increase in binding affinity (see Supporting Information). Instead, these peptides have reduced affinities for pro-survival proteins (Table 1a). Direct binding assays confirmed this observation for two pro-survival proteins, Bcl-x_L and Mcl-1. The penalty imposed by the staple for Bcl-x_L is due to slower on- and faster off-rates (1.8- and 13-fold, respectively). Similarly, the loss in affinity for Mcl-1 resulted predominantly from a faster off-rate (2.8-fold increase, compared to a 1.3-fold reduction in on-rate) (Table 1b).

Inspection of the structure of BimBH3-peptide in complex with Bcl-x_L (PDB code, 3FDL[14]) reveals how the side-chain groups of residues on the exposed face of the peptide form a series of interactions with one another; Glu151 and Glu158 (numbering based on human Bim$_{EL}$) form a pair of salt bridges with Arg154, and the aliphatic methylene moiety of Glu151 packs tightly with the indole side-chain of Trp147. Additionally, Arg154 of Bim forms a water-mediated interaction with Arg103 of Bcl-x_L (Supplementary Figure 3a). Critically, none of these interactions are observed in either structure of the stapled peptides in complex with Bcl-x_L (Supplementary Figure 3b,c).

We have calculated the pairwise interaction energy between the side-chain groups of each of these residues employing the AUTODOCK empirical function: the AUTODOCK potential

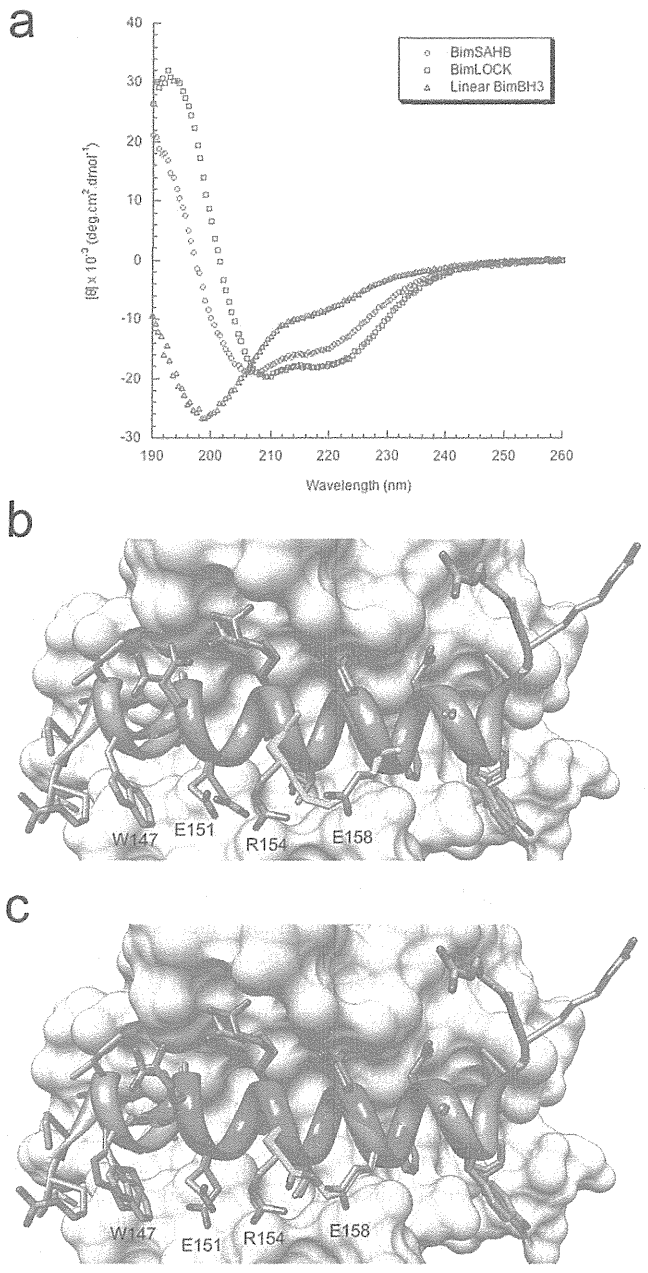

Figure 2. Characterization of constrained BimBH3 peptides. (a) Circular dichroism was used to measure the percentage of helical content for BimSAHB, BimLOCK, and an equivalent linear BimBH3 peptide. Both constrained BimBH3 peptides were found to have significant helical content (BimSAHB 39% helix; BimLOCK 49% helix), while the linear peptide was found to have a modest secondary structure content (21% helix). (b) Structure of the Bcl-x_L:BimSAHB complex overlaid with linear BimBH3 peptide in complex with Bcl-x_L (PDB code, 3FDL;[14] note that the peptide used for the 3FDL structure is longer than those used in this study). Peptide regions of BimSAHB are colored green and the hydrocarbon staple yellow. (c) Structure of the Bcl-x_L:BimLOCK complex overlaid with BimBH3. Peptide regions of BimLOCK are colored magenta and the lactam bridge yellow. BimBH3 is colored blue, and Bcl-x_L is represented in surface format in both complexes. Peptide sequences are as detailed in Table 1 unless otherwise stated.

includes five major contributions to the total free energy of interaction: the van der Waals, hydrogen-bond, electrostatic, conformational entropy, and desolvation energies.[15] The individual energies of interaction calculated were, between Trp147–Glu151, −0.3 kJ mol^{-1}, Glu151–Arg154, −7.0 kJ mol^{-1}, and Arg154–Glu158, −2.7 kJ mol^{-1} (using the Bcl-x_L/Bim coordinates), yielding a total interaction energy between all four residues of −10.0 kJ mol^{-1}. Assuming these side-chains do not interact with one another in the free peptide, the cumulative effect of increased helicity of the peptide and estimated loss in binding energy due to missing side-chain interactions, the anticipated reduction in binding affinity for BimSAHB and BimLOCK is 24-fold and 16-fold, respectively. These estimates compare favorably with the observed 26-fold reduction from the competition assay and 8-fold reduction from the direct binding assay for BimSAHB (Table 1, Supplementary Table 2) and, likewise, 3-fold reduction from the competition assay for BimLOCK.

For Mcl-1 and A1, where the reduction in binding affinity observed by the introduction of the constraint is not as large as that observed for Bcl-2 and Bcl-x_L, either the side-chain groups may maintain some interaction with one another or the side-chain groups may interact with the pro-survival receptor to improve binding affinity. To further assess the contribution of the intramolecular bonding network on the exposed face of the peptide and to ensure loss of affinity could not be attributed to steric hindrance imposed by the staple, we tested the binding affinity of an unstapled Bim peptide (linear Bim with Glu151 and Arg154 substituted with pentenylalanine residues but not subjected to ring closing metathesis) (Table 1b). This peptide bound Bcl-x_L with a further reduced affinity as compared to the stapled Bim, as would be anticipated with the combined effects of a reduction in helicity (due to loss of the staple) and the loss of the stabilizing intramolecular network.

Upon binding their pro-survival receptor, the BH3 peptides adopt an α-helical geometry, stabilized by the interactions between receptor and peptide *and* by the intramolecular interactions within the peptide, specifically the classical hydrogen bond between the carbonyl oxygen and the NH groups (i with $i + 4$) and also the interactions between the side-chain groups. Disrupting the latter of these interactions results in a decrease in binding affinity; in our estimate, this is ~10 kJ mol^{-1} in the case of the BimBH3 peptide. The introduction of the staple into the peptides has two consequences: (i) while the staple is able to preorganize the helix and reduce the entropic penalty for the association, the introduction of a covalent bond between side-chains removes the contribution to the binding energy that comes about when the two residues interact (in the salt bridge formed between Arg154 and Glu158, we estimate this to be 2.7 kJ mol^{-1}), and (ii) the chemical nature of the staple may not be conducive to forming stable interactions with the side-chain group of the residue one turn away. Loss of a stable interaction with the staple can be perpetuated down the chain; in both stapled peptides here, the result is the loss of all stabilizing interactions between side-chains, most critically the loss of the salt-bridge between Glu151 and Arg154. The binding free energy reflects the change in free energy between unbound and bound states, and since the covalent linkage is present in both states, there is no change in free energy of interaction across the staple upon binding. In contrast, in the native peptide, we calculate a significant favorable change in intramolecular energy of the ligand upon binding.

The structures of the peptides in complex with pro-survival Bcl-x_L reveal that they bind analogously to unrestrained BimBH3, neither modification interacting directly with the target protein unlike that observed with another stabilized peptide in complex with Mcl-1[16] where the staple itself makes

Table 1. Analyses of Binding of BimBH3 Peptides to Pro-Survival Proteins Using Biacore-Based Assays

a					
K_i (nM)	Bcl-2	Bcl-x_L	Bcl-w	Mcl-1	A1
BimSAHB	460 ± 80	300 ± 37	370 ± 61	3.4 ± 0.1	4.1 ± 0.3
BimLOCK	800 ± 27	35 ± 3.7	37 ± 3.0	3.7 ± 0.3	4.7 ± 0.1
Linear Bim	6.8 ± 1.6	11 ± 0.6	25 ± 2.3	<1.4	<2.5

b	on-rate K_a (1/Ms)	off-rate K_d (1/s)	affinity K_D
Bcl-x_L			
BimSAHB	3.2×10^6	1.5×10^{-1}	45 nM
unstapled BimSAHB	7.9×10^5	7.5×10^{-2}	95 nM
linear BimBH3	1.7×10^6	1.1×10^{-2}	5.7 nM
Mcl-1			
BimSAHB	3.7×10^6	2.7×10^{-3}	0.73 nM
linear BimBH3	4.9×10^6	9.7×10^{-4}	0.20 nM

c	sequence	note
BimSAHB	Ac-^{145}EIWIAQELRXIGDXFNAYYA^{164}-NH_2	X represents linked (*S*)-pentenylalanine residues
BimLOCK	Ac-^{145}EIWIAQELRRIGDEFNAYYA^{164}-NH_2	R154 and E158 linked by lactam bridge
linear BimBH3	Ac-^{145}EIWIAQELRRIGDEFNAYYA^{164}-NH_2	

(a) Competition experiments performed using a Biacore 3000 as previously described.[20] Values are presented as a K_i in nM, with SD (n = 3 independent experiments). (b) Direct affinity measurements for binding of linear BimBH3 and BimSAHB to Bcl-x_L and Mcl-1. Measurements were performed using a BIAcore S51. Peptides were passed over a sensor chip to which either recombinant Bcl-x_L-GST or Mcl-1-GST fusion proteins had been coupled via an anti-GST antibody. Direct association and dissociation rates were measured at a range of concentrations from which K_D values were calculated. Unstapled BimSAHB refers to a BimSAHB peptide in which pentylalanine residues have not been linked. (c) Sequences for peptides.

intimate hydrophobic contact with the side-chain of Phe318, and one of the flanking α-disubstitution methyl groups contacts Gly262. Unexpectedly, enhanced helicity did not improve activity with regards to affinity for the pro-survival proteins or bioactivity, as measured by induction of cytochrome *c* release from mitochondria and cellular uptake. Our findings recapitulate earlier observations[17,18] that stapling of peptides to enforce helicity does not necessarily impart enhanced binding affinity for target proteins and support the notion that interactions between the staple and target protein may be required for high affinity interactions in some circumstances.[19] Thus, the design of stapled peptides should consider how the staple might interact with both the target *and* the rest of the peptide, and particularly in the latter case whether its introduction might disrupt otherwise stabilizing interactions.

In conclusion, we undertook an investigation of stapled peptides as part of our on going studies into the mechanism of the Bcl-2 family of proteins. We found that the addition of a hydrocarbon staple to the BimBH3 peptide, either via Grubbs metathesis or formation of an external amide bond, does not change the peptide-like properties of the molecules in a manner that makes them significantly more drug-like. While modification of peptides may yet prove beneficial for drug development, in this case, we describe that the addition of external constraints does not enhance either binding affinity or cell permeability.

METHODS

Circular Dichroism Measurements. Circular dichroism was used to measure the percentage of helical content for BimSAHB, BimLOCK, and an equivalent linear BimBH3 peptide. Spectra were performed on 50 μM peptide solutions in 0.1 M potassium phosphate (pH 7) at 25 °C. Percent helicity was calculated as previously described.[22,23]

Structure Determination. Bcl-x_L protein preparation, crystallization, and structure determination for both the Bcl-x_L:BimSAHB complex and the Bcl-x_L:BimLOCK complex were as previously described for the Bcl-x_L:BimBH3 complex.[14] Crystallographic statistics for the two complexes are reported in Supplementary Table 1.

Cytochrome *c* Release. Cells were pelleted and lysed in 0.025% (w/v) digitonin containing lysis buffer (20 mM Hepes, pH 7.2, 100 mM KCl, 5 mM $MgCl_2$, 1 mM EDTA, 1 mM EGTA, and 250 mM sucrose, supplemented with Complete Protease Inhibitor Cocktail from Roche). The crude lysates, containing mitochondria, were incubated with or without 1% (w/v) Triton-X100 or increasing concentrations of Bim peptides for 1 h at 30 °C, pelleted at 4000 rpm at 4 °C for 15 min, and the supernatant collected. The amount of released cytochrome *c* was determined by ELISA (R&D systems), according to the manufacturer's protocol.

BIAcore Competition Assays. BIAcore competition assays were performed as previously described.[20,21] Pro-survival proteins (5 nM) (Bcl-2, Bcl-x_L, and Bcl-w prepared as described in ref , Mcl-1 prepared as described in ref 24, A1 prepared as described in ref 25) were incubated with increasing concentrations of BimBH3 peptides for 2 h in running buffer prior to injection onto a CM5 chip onto which either a wild-type 26-mer BimBH3 peptide or an inert BimBH3 mutant peptide (Bim4E) was immobilized.

Direct Affinity Measurements. Direct binding assays were performed with a Biacore S51 as previously described.[9] Briefly, anti-GST antibody was immobilized to a CM5 chip using amine coupling. Recombinant GST-tagged Bcl-x_L or GST-tagged Mcl-1 (100 μg mL^{-1}) was captured to the chip followed by injection of peptide at a variety of concentrations. Sensograms were generated by subtracting the binding response from that of a reference spot to which GST alone had been captured.

Killing Assays. MEFs were trypsinized, collected, and then washed twice in serum-free media followed by plating of cells (5×10^4/well) in 50 μL, exposed to BimSAHB (20 μM) or vehicle in serum-free media for 2 h, and serum replacement (20% (v/v) serum in 50 μL media) for an overall treatment duration as indicated.

Colony Survival Assays. Retroviruses encoding BH3-only proteins were transduced as described.[20] Infected MEFs (GFP(+) cells) were sorted by FACS and long-term assays of colony formation performed as described.[20]

Molecular Modeling. The free energy of interaction between the side-chain groups on the BimBH3-peptide was calculated using the AUTODOCK function.[15] In its original formulation, the AUTODOCK potential (model C) includes terms that represent the entropic

dx.doi.org/10.1021/cb3005403 | ACS Chem. Biol. XXXX, XXX, XXX–XXX

penalty for restriction of conformational freedom and desolvation of the ligand only. Here, we have included these two components for both molecular constituents and consequently reduced the contribution to the total free energy of interaction of each by half. The AMBER all-atom partial atomic charges[26] were used to calculate the electrostatic interaction energy. Hydrogen atoms were added to fill valencies using the UCSF Chimera package.[27]

Detailed methods for peptide synthesis, structure determination, K_i calculations, and binding analysis are provided in the Supporting Information.

■ ASSOCIATED CONTENT

Supporting Information

BimSAHB peptide does not kill MEFs; reconstituted $Bax^{-/-}Bak^{-/-}$ MEF cells express comparable levels of wild-type Bax and Bax K21E. This material is available free of charge via the Internet at http://pubs.acs.org.

Accession Codes

Atomic coordinates and structure factors have been deposited in the Protein Data Bank (PDB ID codes, 2YQ6 for Bcl-xL:BimSAHB and 2YQ7 for Bcl-xL:BimLOCK).

■ AUTHOR INFORMATION

Corresponding Author

*E-mail: Brian.Smith@latrobe.edu.au (B.J.S.); deshayes.kurt@gene.com (K.D.); czabotar@wehi.edu.au (P.E.C.).

Notes

The authors declare the following competing financial interest(s): Genentech is a member of the Roche Group. Roche Pharma and Aileron Therapeutics have an independent collaboration developing stapled peptide technology. Between 2007 and 2010, the Walter and Eliza Hall Institute of Medical Research had a research collaboration agreement with Genentech and Abbott in the field of apoptosis, specifically the Bcl-2 protein family.

■ ACKNOWLEDGMENTS

We thank A. Georgiou, H. Ierino, G. Thompson, and A. Wardak for outstanding technical assistance, P. M. Colman for advice and assistance with manuscript preparation, our colleagues J. Adams, A. Cochran, S. Cory, J. Babon, and V. Dixit for useful discussions, and Abbott Laboratories for ABT-737. This work was supported by fellowships and grants from the Australian Research Council (ARC) (fellowships to T.O. and P.E.C.), the National Health and Medical Research Council (NHMRC) (fellowship to D.C.S.H.; project grants 575561 to P.E.C. and 637360 to P.E.C. and D.C.S.H.; program grants 461221 and 1016701), the Leukemia and Lymphoma Society (LLS) (SCOR 7413), and the Australian Cancer Research Foundation. Infrastructure support from a NHMRC IRIISS grant #361646 and a Victorian State Government OIS grant is gratefully acknowledged (by T.O., H.Y., B.J.S., D.C.S.H, and P.E.C.). X-ray data were collected at the Australian Synchrotron, with assistance from the staff of the macromolecular beamlines.

■ REFERENCES

(1) Tyndall, J. D., Nall, T., and Fairlie, D. P. (2005) Proteases universally recognize beta strands in their active sites. *Chem. Rev. 105*, 973−999.

(2) Bird, G. H., Bernal, F., Pitter, K., and Walensky, L. D. (2008) Synthesis and biophysical characterization of stabilized alpha-helices of BCL-2 domains. *Methods Enzymol. 446*, 369−386.

(3) Walensky, L. D., Kung, A. L., Escher, I., Malia, T. J., Barbuto, S., Wright, R. D., Wagner, G., Verdine, G. L., and Korsmeyer, S. J. (2004) Activation of apoptosis *in vivo* by a hydrocarbon-stapled BH3 helix. *Science 305*, 1466−1470.

(4) Moellering, R. E., Cornejo, M., Davis, T. N., Del Bianco, C., Aster, J. C., Blacklow, S. C., Kung, A. L., Gilliland, D. G., Verdine, G. L., and Bradner, J. E. (2009) Direct inhibition of the NOTCH transcription factor complex. *Nature 462*, 182−188.

(5) LaBelle, J. L., Katz, S. G., Bird, G. H., Gavathiotis, E., Stewart, M. L., Lawrence, C., Fisher, J. K., Godes, M., Pitter, K., Kung, A. L., and Walensky, L. D. (2012) A stapled BIM peptide overcomes apoptotic resistance in hematologic cancers. *J. Clin. Invest. 122*, 2018−2031.

(6) Walensky, L. D., Pitter, K., Morash, J., Oh, K. J., Barbuto, S., Fisher, J., Smith, E., Verdine, G. L., and Korsmeyer, S. J. (2006) A stapled BID BH3 helix directly binds and activates BAX. *Mol. Cell 24*, 199−210.

(7) Oltersdorf, T., Elmore, S. W., Shoemaker, A. R., Armstrong, R. C., Augeri, D. J., Belli, B. A., Bruncko, M., Deckwerth, T. L., Dinges, J., Hajduk, P. J., Joseph, M. K., Kitada, S., Korsmeyer, S. J., Kunzer, A. R., Letai, A., Li, C., Mitten, M. J., Nettesheim, D. G., Ng, S., Nimmer, P. M., O'Connor, J. M., Oleksijew, A., Petros, A. M., Reed, J. C., Shen, W., Tahir, S. K., Thompson, C. B., Tomaselli, K. J., Wang, B., Wendt, M. D., Zhang, H., Fesik, S. W., and Rosenberg, S. H. (2005) An inhibitor of Bcl-2 family proteins induces regression of solid tumours. *Nature 435*, 677−681.

(8) Gavathiotis, E., Suzuki, M., Davis, M. L., Pitter, K., Bird, G. H., Katz, S. G., Tu, H. C., Kim, H., Cheng, E. H., Tjandra, N., and Walensky, L. D. (2008) BAX activation is initiated at a novel interaction site. *Nature 455*, 1076−1081.

(9) Lee, E. F., Chen, L., Yang, H., Colman, P. M., Huang, D. C., and Fairlie, W. D. (2008) EGL-1 BH3 mutants reveal the importance of protein levels and target affinity for cell-killing potency. *Cell Death Differ. 15*, 1609−1618.

(10) Willis, S. N., and Adams, J. M. (2005) Life in the balance: How BH3-only proteins induce apoptosis. *Curr. Opin. Cell Biol. 17*, 617−625.

(11) Dai, H., Smith, A., Meng, X. W., Schneider, P. A., Pang, Y. P., and Kaufmann, S. H. (2011) Transient binding of an activator BH3 domain to the Bak BH3-binding groove initiates Bak oligomerization. *J. Cell Biol. 194*, 39−48.

(12) Skelton, N. J., Chen, Y. M., Dubree, N., Quan, C., Jackson, D. Y., Cochran, A., Zobel, K., Deshayes, K., Baca, M., Pisabarro, M. T., and Lowman, H. B. (2001) Structure-function analysis of a phage display-derived peptide that binds to insulin-like growth factor binding protein 1. *Biochemistry 40*, 8487−8498.

(13) Yang, B., Liu, D., and Huang, Z. (2004) Synthesis and helical structure of lactam bridged BH3 peptides derived from pro-apoptotic Bcl-2 family proteins. *Bioorg. Med. Chem. Lett. 14*, 1403−1406.

(14) Lee, E. F., Sadowsky, J. D., Smith, B. J., Czabotar, P. E., Peterson-Kaufman, K. J., Colman, P. M., Gellman, S. H., and Fairlie, W. D. (2009) High-resolution structural characterization of a helical alpha/beta-peptide foldamer bound to the anti-apoptotic protein Bcl-x(L). *Angew. Chem., Int. Ed. 48*, 4318−4322.

(15) Morris, G. M., Goodsell, D. S., Halliday, R. S., Huey, R., Hart, W. E., Belew, R. K., and Olson, A. J. (1998) Automated docking using a Lamarckian genetic algorithm and an empirical binding free energy function. *J. Comput. Chem. 19*, 1639−1662.

(16) Stewart, M. L., Fire, E., Keating, A. E., and Walensky, L. D. (2010) The MCL-1 BH3 helix is an exclusive MCL-1 inhibitor and apoptosis sensitizer. *Nat. Chem. Biol. 6*, 595−601.

(17) Marshall, G. R., Kuster, D. J., and Che, Y. (2009) Chemogenomics with protein secondary-structure mimetics. *Methods Mol. Biol. 575*, 123−158.

(18) Martin, S. F. (2007) Preorganization in biological systems: Are conformational constraints worth the energy? *Pure Appl. Chem. 79*, 193−200.

(19) Joseph, T. L., Lane, D., and Verma, C. S. (2010) Stapled peptides in the p53 pathway: Computer simulations reveal novel

interactions of the staples with the target protein. *Cell Cycle 9*, 4560–4568.

(20) Chen, L., Willis, S. N., Wei, A., Smith, B. J., Fletcher, J. I., Hinds, M. G., Colman, P. M., Day, C. L., Adams, J. M., and Huang, D. C. S. (2005) Differential targeting of pro-survival Bcl-2 proteins by their BH3-only ligands allows complementary apoptotic function. *Mol. Cell 17*, 393–403.

(21) Lee, E. F., Czabotar, P. E., van Delft, M. F., Michalak, E., Boyle, M., Willis, S. N., Puthalakath, H., Bouillet, P., Colman, P. M., Huang, D. C. S., and Fairlie, W. D. (2008) A novel BH3 ligand that selectively targets Mcl-1 reveals that apoptosis can proceed without Mcl-1 degradation. *J. Cell Biol. 180*, 341–355.

(22) Jackson, D. Y., King, D. S., Chmielewski, J., Singh, S., and Schultz, P. G. (1991) General approach to the synthesis of short alpha-helical peptides. *J. Am. Chem. Soc. 113*, 9391–9392.

(23) Kumita, J. R., Smart, O. S., and Woolley, G. A. (2000) Photo-control of helix content in a short peptide. *Proc. Natl. Acad. Sci. U.S.A. 97*, 3803–3808.

(24) Czabotar, P. E., Lee, E. F., van Delft, M. F., Day, C. L., Smith, B. J., Huang, D. C., Fairlie, W. D., Hinds, M. G., and Colman, P. M. (2007) Structural insights into the degradation of Mcl-1 induced by BH3 domains. *Proc. Natl. Acad. Sci. U.S.A. 104*, 6217–6222.

(25) Smits, C., Czabotar, P. E., Hinds, M. G., and Day, C. L. (2008) Structural plasticity underpins promiscuous binding of the pro-survival protein A1. *Structure 16*, 818–829.

(26) Yang, L., Tan, C.-H., Hsieh, M.-J., Wang, J., Duan, Y., Cieplak, P., Caldwell, J., Kollman, P. A., and Luo, R. (2006) New-generation amber united-atom force field. *J. Phys. Chem. B 110*, 13166–13176.

(27) Pettersen, E. F., Goddard, T. D., Huang, C. C., Couch, G. S., Greenblatt, D. M., Meng, E. C., and Ferrin, T. E. (2004) UCSF Chimera: A visualization system for exploratory research and analysis. *J. Comput. Chem. 25*, 1605–1612.

dx.doi.org/10.1021/cb3005403 | *ACS Chem. Biol.* XXXX, XXX, XXX–XXX